THE OXIDATION OF IRON BY LEAD OXIDE - SILICA MELTS

by

BERNARD PORTIER

A THESIS SUBMITTED IN PARTIAL FULFILMENT OF THE REQUIREMENTS FOR THE DEGREE OF MASTER OF APPLIED SCIENCE

in the Department of METALLURGY

We accept this thesis as conforming to the standard required from candidates for the degree of MASTER OF APPLIED SCIENCE

Members of the Department of Metallurgy

The University of British Columbia
March, 1967

In presenting this thesis in partial fulfilment of the requirements for an advanced degree at the University of British Columbia, I agree that the Library shall make it freely available for reference and study. I further agree that permission for extensive copying of this thesis for scholarly purposes may be granted by the Head of my Department or by his representatives. It is understood that copying or publication of this thesis for financial gain shall not be allowed without my written permission.

Department of Metallurgy

The University of British Columbia
Vancouver 8, Canada

Date April 25, 1967

Resumé

L'oxydation du fer par des laitiers constitués de silice et d'oxyde de plomb a fait l'objet d'une étude expérimentale pour un large intervalle de composition entre 850 et 1000°C. Les vitesses de réaction ont été obtenues par des mesures de résistance électrique. Dans le domaine de composition massique 80-88 % de PbO, la vitesse d'oxydation est proportionnelle à la fraction molaire d'oxyde de plomb dans le bain, c'est-à-dire à la concentration en cations Pb^{++}. On suppose donc que la vitesse de réaction est limitée par le transfert d'électrons entre les ions métalliques contrairement à la réaction d'oxydation du carbone par les mêmes laitiers dans laquelle interviennent les ions oxygène.

L'énergie apparente d'activation est de 50 ± 7 Kcal/mole.

Deux séries de différentes valeurs d'activité pour le système binaire $PbO-SiO_2$ ont été utilisées et sont comparées à la lumière de la présente étude.

ABSTRACT

An investigation of the oxidation of solid iron by lead oxide-silica melts was undertaken between 850°C and 1000°C over a wide range of oxidising potentials. The experimental reaction rates were measured by a technique of electrical resistance measurements. In the intermediate range of concentration investigated (80-88 % wgt.PbO) the rate of oxidation was found to be proportional to the mole fraction of lead oxide in the melt, in other words, to the lead ion concentration. The rate determining step of iron oxidation by lead oxide-silica melts is supposed to involve lead cations in contrast with the oxidation of carbon where oxygen ions are involved.

The apparent activation energy was found to be 50 ± 7 Kcal/mole.

Two sets of activity data concerning the lead oxide in $PbO-SiO_2$ melts were available and were compared by processing the present results on iron oxidation and previous results on carbon oxidation by similar melts.

ACKNOWLEDGEMENT

The author wishes to express his gratitude for the valuable assistance rendered by the members of the Department of Metallurgy throughout this work. Sincere appreciation is especially extended to Dr.C.S. Samis who directed this investigation and to Dr. E.Peters for many useful discussions of this work.

The author is also particularly indebted to the Canada Council for a Scholarship which made this study possible.

TABLE OF CONTENTS

LIST OF FIGURES

LIST OF TABLES

INTRODUCTION

Slag-metal systems are often dealt with in industrial practice and they have been frequently investigated. Most studies, however, concern liquid systems and little attention has been focussed on heterogeneous reactions between solid metal and liquid phases. The study of the latter type of reactions is, in the case of oxidation, a reasonable approach to a better understanding of the molten state, since the gaseous oxidation of metals is better known than the oxidation reactions in molten systems.

The present work on the oxidation of solid iron by lead oxide-silica melts has been undertaken in order to study the kinetics of the reaction and to draw comparisons with previous studies on similar systems[1,2].

It is advantageous first to consider the present knowledge on the gaseous oxidation of iron and then the available results about oxidation by oxidising melts.

Kinetics of the Gaseous Oxidation of Metals

The kinetics of the gaseous oxidation of iron have been investigated by various authors[3,4,5,6,7]. Both the chemical interface reaction and diffusion through the oxide scale can be rate determining. Linear reaction rates can be observed[3,4] and the corresponding rate constants are dependent on the pressure of the oxidising gas[4,5]; in the case of CO_2 a linear dependence has been found[3]. The corresponding

activation energy was found to be 60 KCal/mole in the case of carbon dioxide[3] and 16 KCal/mole in the case of oxygen at low pressure[5].

In contrast to this, parabolic reaction rates are generally observed and correspond to a reaction controlled by the diffusion of atoms or point defects in the external oxide layers[3]. The oxygen pressure dependence varies with the nature of the oxide layer. If magnetite is produced, the oxygen pressure has no effect on the reaction rate[4,6]. If only wustite is produced, the oxygen pressure has a positive effect on the reaction rates[4,5,7]. The activation energy corresponding to the diffusion of iron in a wustite layer is 30 KCal/mole[3,5].

Kinetics of Oxidation by Oxidising Melts

As an example of oxidation of solid metals by oxidizing melts, an investigation on solid iron was made[9], and an activation energy of 72 KCal/mole was obtained for the reaction: $Fe + [Fe_2O_3] \rightleftharpoons 3[FeO]$. In this connection, the electrochemical studies of oxidising melts show that the physico-chemical properties of slags are closely related to the oxygen potential of the system[10,11,12].

The oxidation of solid carbon by lead oxide-silica melts has been investigated by several authors[1,2,8]. It was shown that the rate determining species is oxygen ions, and that the rate of oxidation is proportional to the geometric surface area of carbon and to the oxygen potential of the binary melts[1] or to the square of the oxygen ion concentration of the ternary melts[2]. The activation energy was found to be independent of the nature of carbon[2]. This suggests that the carbon

oxidation is rate controlled by the melt rather than by the solid phase.

Object and Scope of the Present Investigation

The object of the present work is to study the oxidation kinetics of solid iron in lead oxide-silica melts. Its main purpose is to compare the kinetics of two similar systems: solid iron-molten slag and solid carbon-molten slag, the latter being known from previous works[1,2].

The experimental technique consists in measuring the electrical resistance of an iron wire. A similar technique has been previously described[13].

The lead oxide-silica slags are low melting phases (70%-93% Wgt PbO) (Fig. 1), so that a large range of oxidising melts and temperatures is available experimentally.

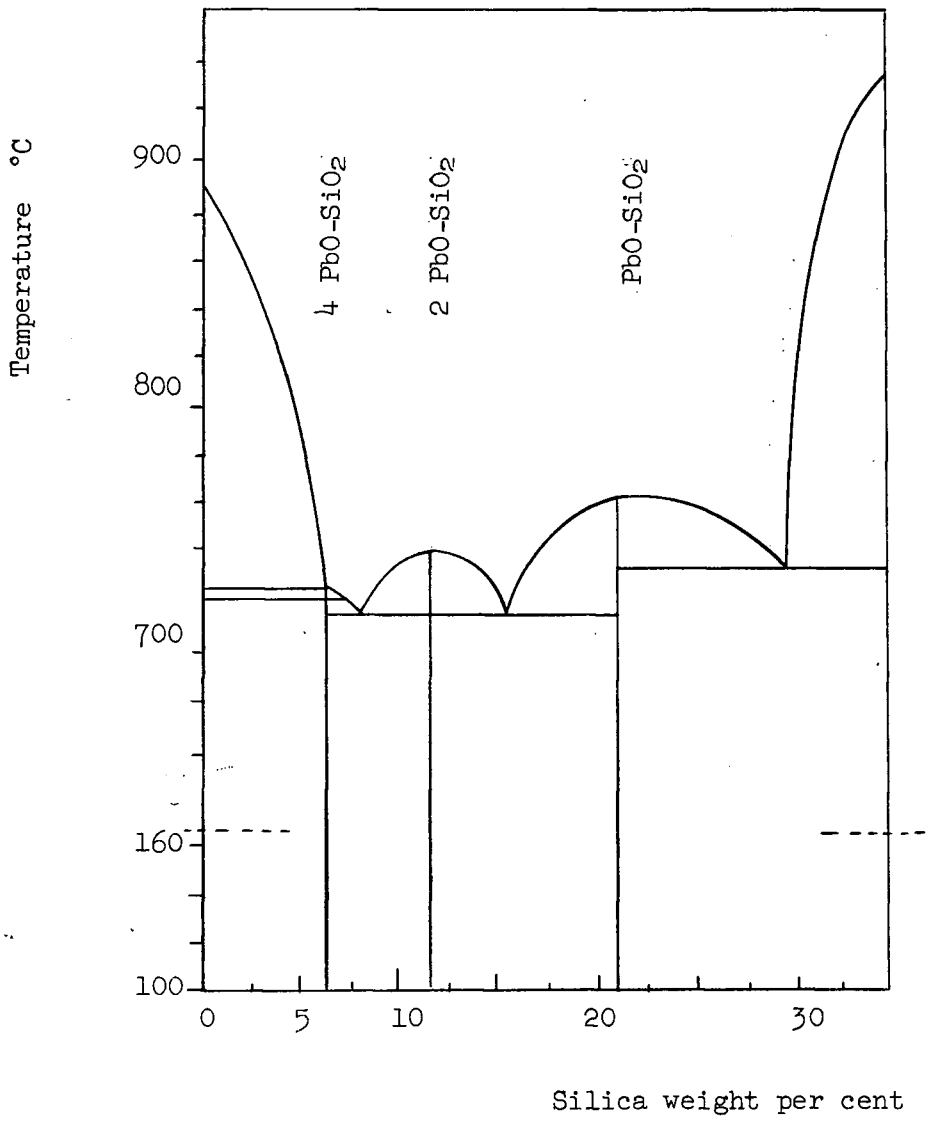

Fig.1 : $PbO-SiO_2$ Phase diagram.

EXPERIMENTAL

Apparatus

The experimental set-up is shown schematically in Fig. 2. An alternative set-up is shown in Fig. 3 and offers two improvements: the possibility of establishing a neutral atmosphere and a better temperature control.

The lower part of the iron wire S constitutes the sample, delimited by the two points where stainless steel leads used for potential reading are spot welded. The main electrical circuit consisted of a battery, an amperemeter, a variable resistor for current adjusting and a standard resistor with potentiometer reading in order to control precisely the intensity of the current.

Materials

Lead oxide Mono (General Chemical Division) and silica powder (Fisher) of reagent grade were used throughout.

The iron was commercial iron wire of the following composition (%):

C	Mn	S	Si	Cr
.03	.2	.04	.I	.I

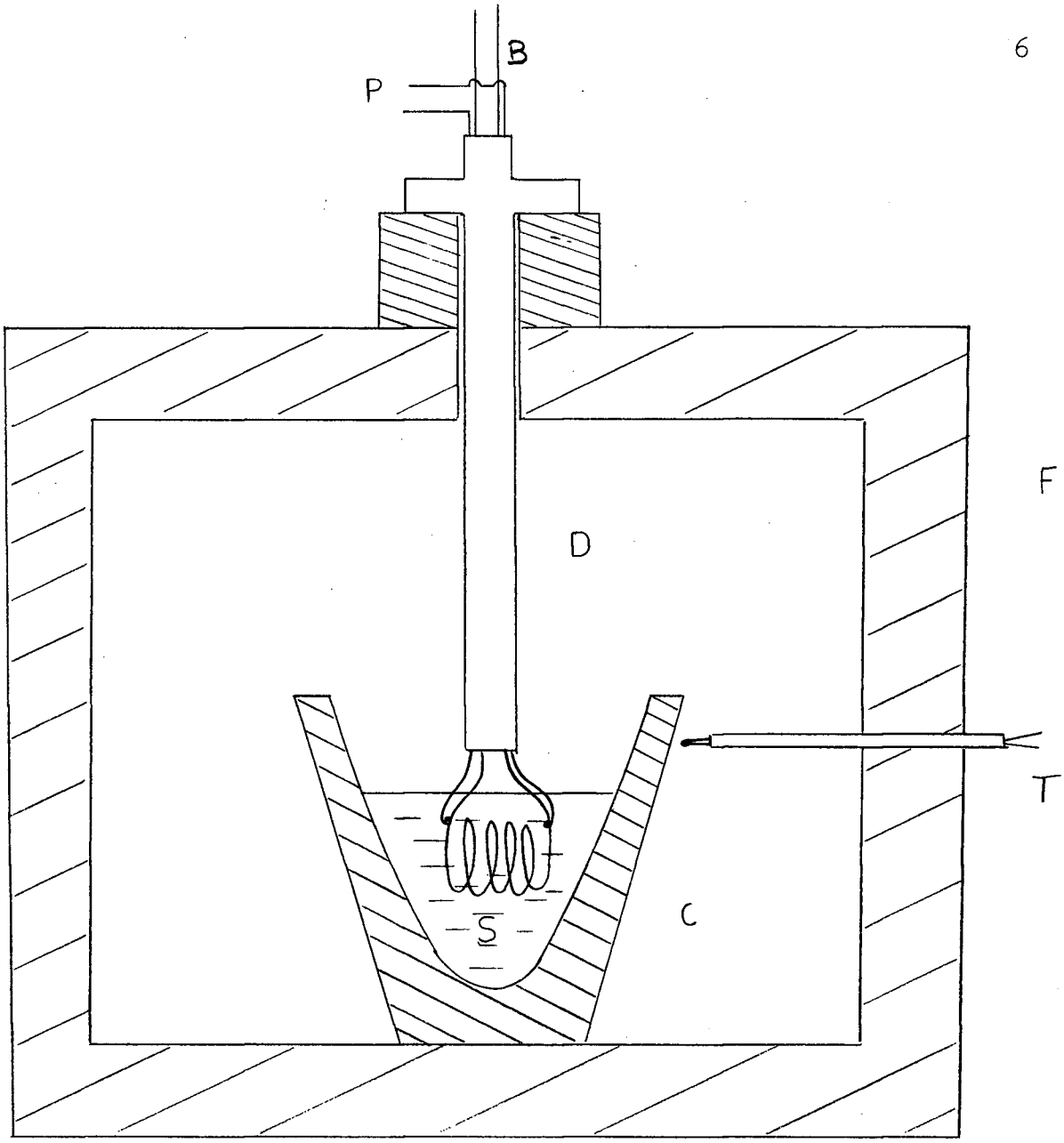

Fig.2: Experimental set-up.

F: Globar Furnace
T: Chromel-Alumel thermocouple connected to a Wheelco controller
C: Fireclay crucible
D: Four hole porcelaine pipe
B: Iron wire connected to the main circuit
P: Stainless steel wire connected to a potentiometer.

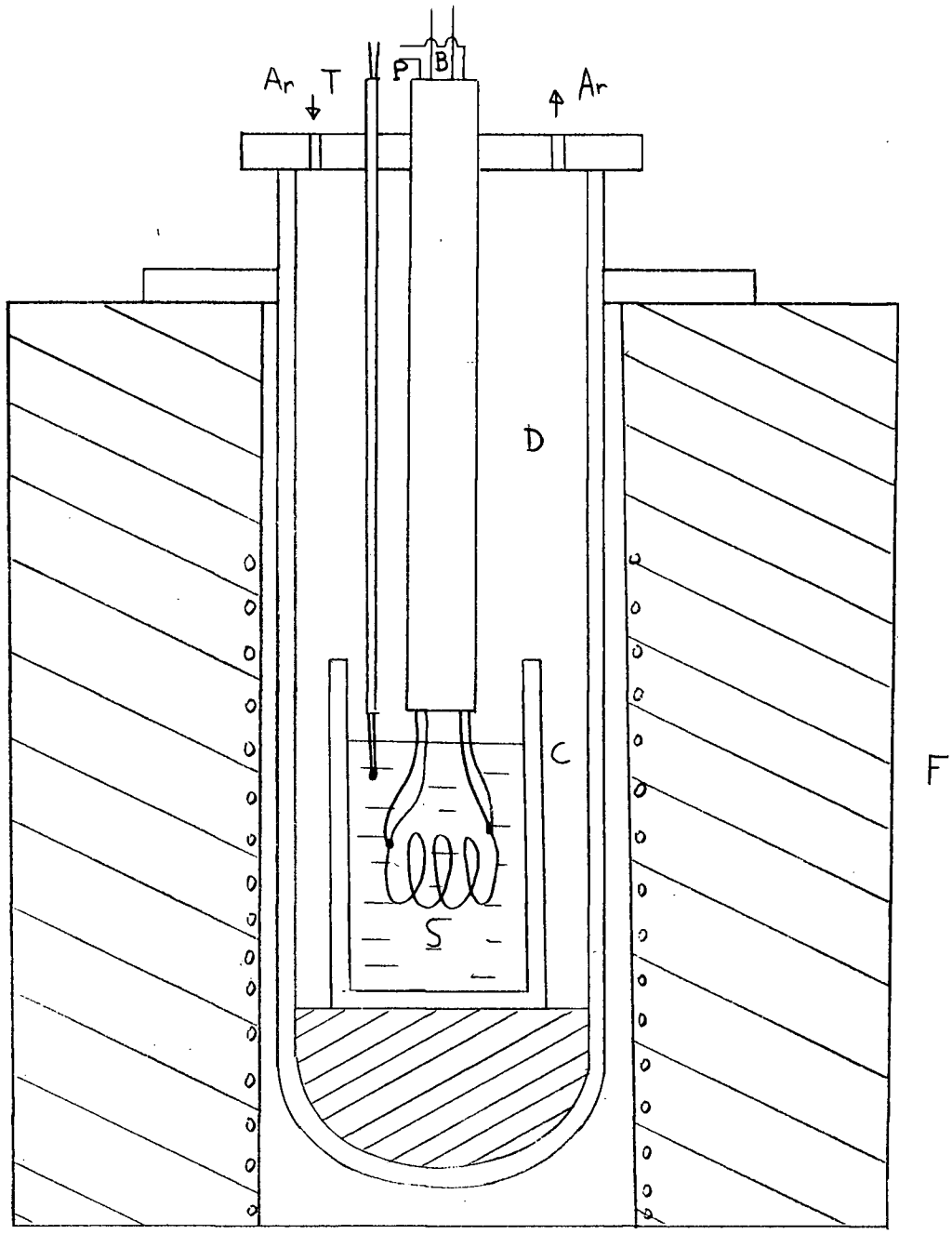

Fig.3: Alternative experimental set-up.

F: Electrical resistor furnace
T: Chromel-Alumel thermocouple connected to a Wheelco controller
C: Zirconia crucible
B: Iron wire
P: Stainless steel leads
Ar: Argon flow.
D: Four hole porcelaine pipe.

Procedure

(1) Preparation of the Samples.

The slag mixtures were prepared in 400 gm batches by weighing suitable amounts of reagents and mixing them manually.

The iron wire was cleaned with emery paper over a length of 3, 6, or 12 inches.

Two stainless steel leads for potential measurements were spot welded at the ends of the desired sample, the cleaned part of the iron wire was spiral shaped and the four vertical leads were protected in a four hole porcelaine holder. The resistance of the sample was then checked at room temperature.

(2) Stages of a Run.

400 gm of slag mixture were placed in a fire clay crucible and heated up in the Globar furnace as shown in the following table:

Time (hours)	heat rate (°C/hour)
1	300-400
2	150
3	100
4-7	0

After sufficient homogeneisation (2-3 hours) at the desired temperature (850°C-1000°C) the wire at room temperature was plundged into the melt.

The potential at the ends of the sample was measured every minute. At the end of a run the wire was lifted and quenched to room temperature.

PRELIMINARY CALCULATIONS

Reaction Rate

The mass of iron unreacted can be calculated from the measure of the electrical resistance of the sample, assuming that the attack of the cylindrical wire is uniform:

Resistance: $$R = \frac{V}{I} = \frac{\rho \ell}{\pi r^2}$$

mass: $$M = \pi r^2 \ell d$$

$$M = \frac{\rho \ell^2 d I}{V} = \frac{K}{V}$$

where

r = radius of the sample (cm)

ℓ = length (cm)

d = density

V = potential at the ends of the sample (v)

I = current intensity (kept constant) (Amp)

K = constant for given I and T.

The surface area A is proportional to the radius of the cylindrical wire, and the mass M to the square of the radius; therefore, the reaction rate expressed in mass unit/surface area unit x time unit is functionally similar to the radius of the wire:

$$r = \sqrt{\frac{\rho \ell I}{\pi V}} = \sqrt{\frac{M}{\pi \ell d}} \qquad (1)$$

A study of the error on the reaction rate calculated by this method is presented in appendix 1. The reaction rate being measured as the derivative of the radius (slope of the curve: radius versus time), relative accuracy is more important than absolute accuracy and the variations of the parameters

included in equation (1) will be taken into account in the range of temperature investigated (850-1000°C).

Temperature Dependence of the Parameters

I. Current I

The current was kept constant by means of a variable carbon plate resistor and was controlled by potential reading at the ends of a standard manganin resistor. The most suitable current for the present set up was 0.25 Amp.

2. Length of the Sample

The length of the sample is considered to be constant in the range of temperature investigated (850-1000°C), the linear expansion of iron being 0.25% in this range.

3. Electrical Resistivity

The temperature dependence of the resistivity of the iron wire was determined in an argon atmosphere in the experimental set-up shown in Fig. 3. A linear dependence is found in the range of temperature 850-1000°C (Fig. 4 and 5A) and a mean linear dependence of the coefficient K is shown in Fig. 5B.

Table 1 gives the values of K at 850°C for three lengths of sample. K' defined by $r^2 = K' \times M$ is independent of temperature.

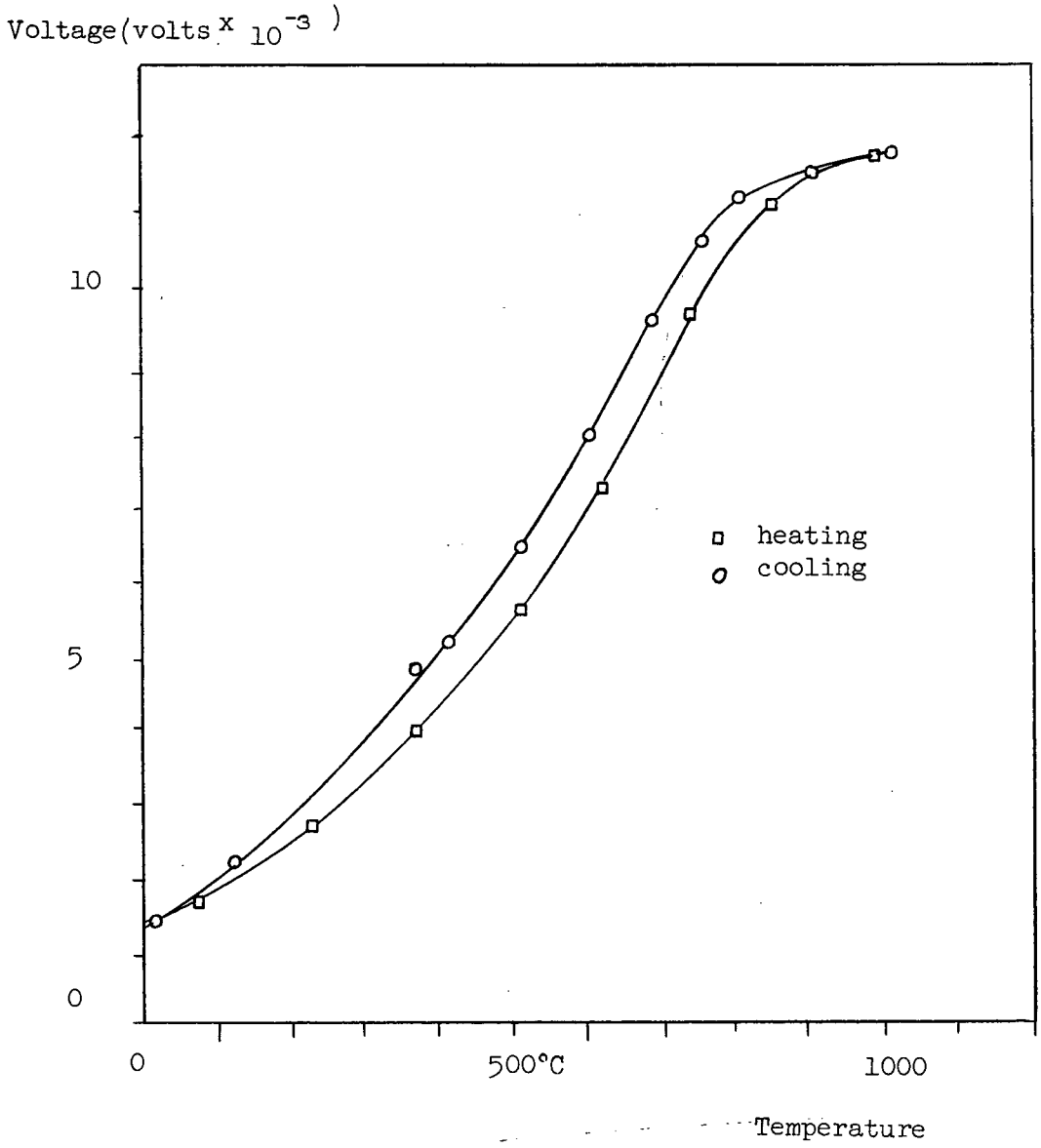

Fig. 4 : Temperature dependence of the iron conductivity.

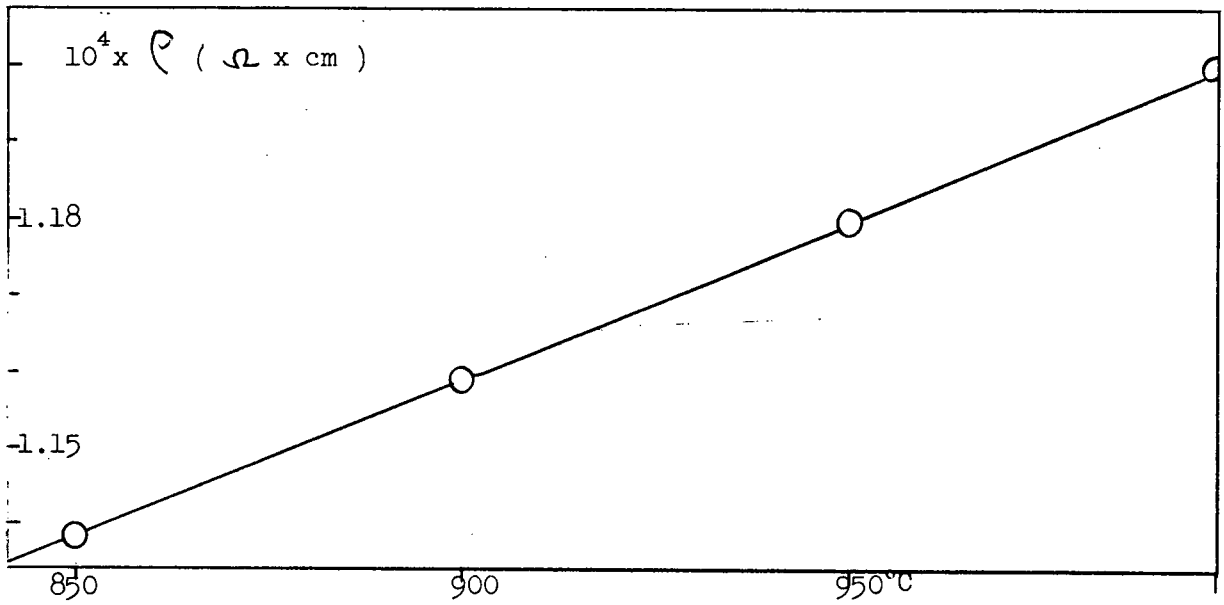

Fig. 5A : Iron wire conductivity (± 0.03).

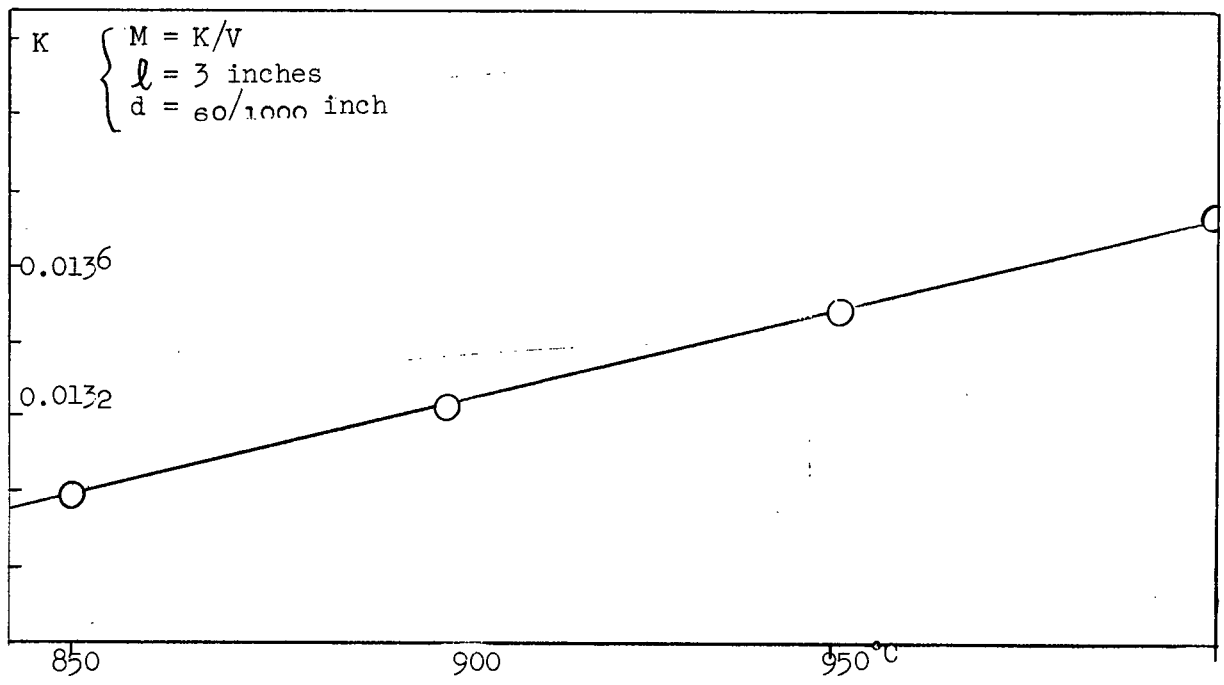

Fig.5B : Temperature dependence of the coefficient K.

ℓ inches	K	K′
3	0.0278	53×10^{-4}
6	0.0511	26.5×10^{-4}
12	0.02045	13.25×10^{-4}

Table 1: Rate calculation coefficients
(T = 850°C, I = 1/4 Amp.)

Oxygen Potential of $PbO-SiO_2$ Slags

In the binary system $PbO-SiO_2$ the oxygen pressure in equilibrium with the lead oxide in the melt is directly proportional to the square of the lead oxide activity[2]. Two sets of activity data are available from studies by Richardson[14] and Kozuka[15]. By extrapolating their data as shown in appendices 2 and 3, two $(aPbO)^2$ scales are obtained for each temperature (Fig. 6 and 7).

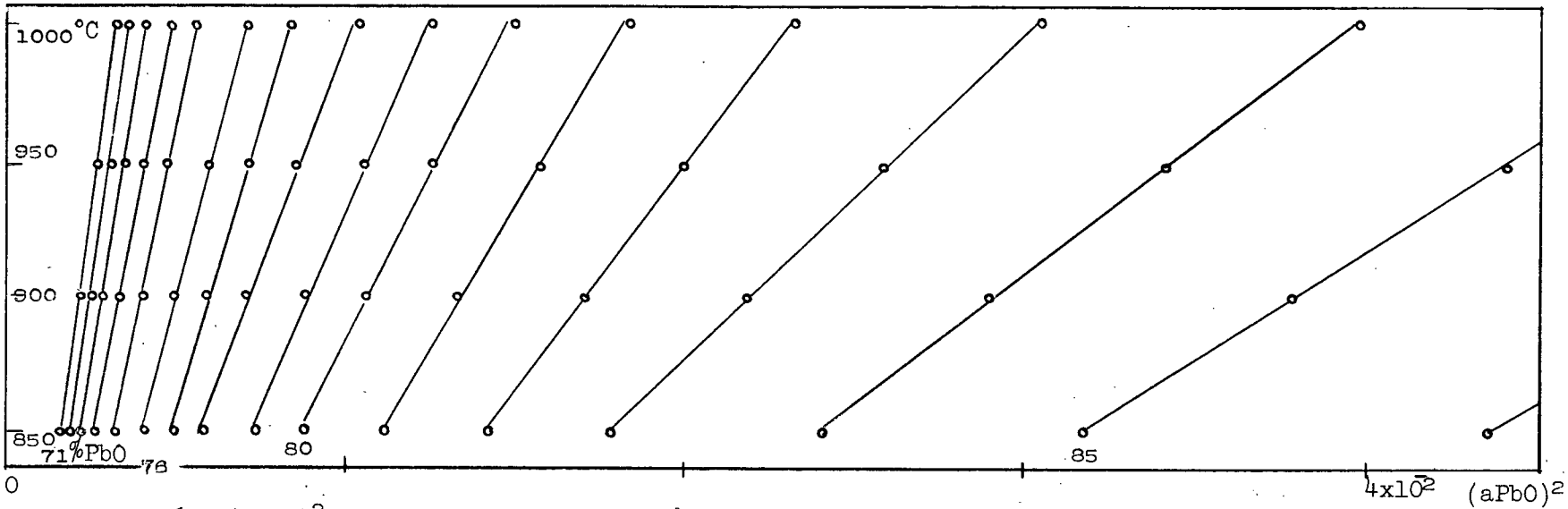

Fig.6 : $(aPbO)^2$ scale from Richardson's data.

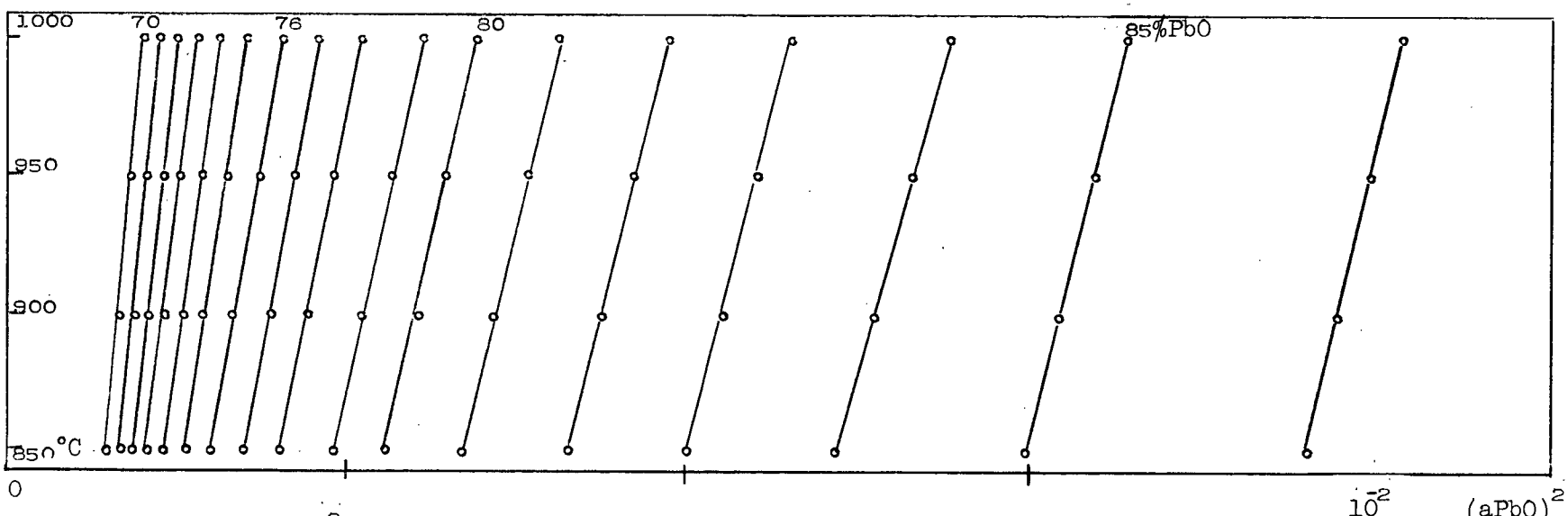

Fig. 7 : $(aPbO)^2$ scale from Kozuka's data.

RESULTS

A. Kinetics for a Given Melt at Fixed Temperature

(1) Linear Reaction Rate

In general every experiment displays two reaction rate stages (Fig. 8): A short stage of low rate (0-12 minutes), more or less linear, and a longer stage of linear rate. The latter stage corresponds to a fairly regular attack of the cylindrical wire as revealed by examination of the sample. Its slope (cm/min) is a measure of the reaction rate. Some experiments also display a final stage of fast, non linear rate (Fig. 8) corresponding to an irregular attack of the wire resulting in apparently high rates.

(2) Reproducibility

A reproducibility of ± 20% is generally observed for rate measurements.

(3) Diffusion

Reciprocation of the sample did not exert any significant effect on the reaction rate, and this leads to the conclusion that neither the diffusion of Pb ions nor the diffusion of Fe ions through a boundary layer can be rate-determining under these experimental conditions.

B. Oxidation Reaction Rates for Various Melts at Different Temperatures

The experimental reaction rates are presented in Table 2. In high lead oxide melts (>86% PbO) the experimental scatter increased with

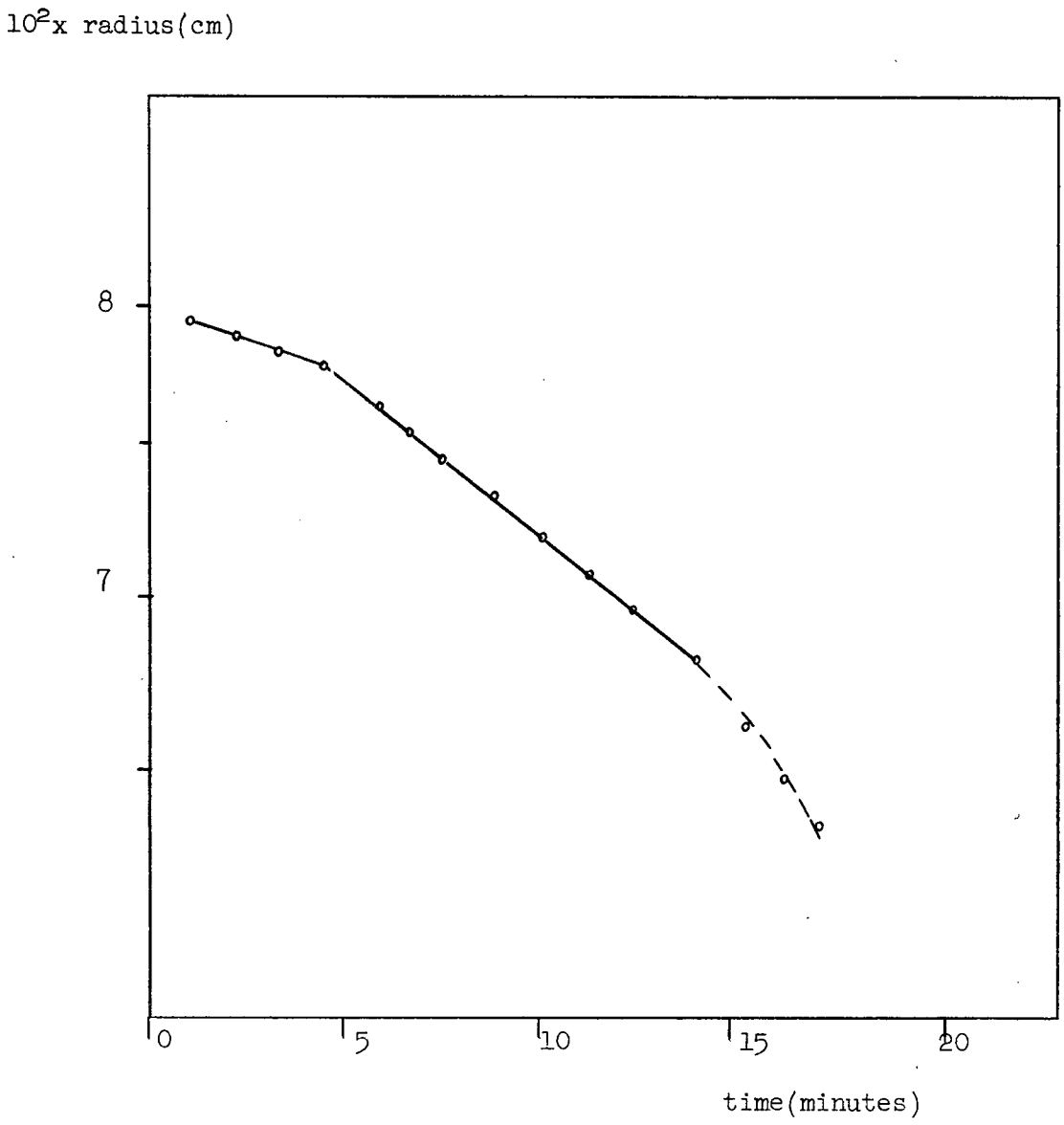

Fig. 8 : Example of a typical experimental rate curve.

temperature to such an extent (± 50 %) that the observed rates were not considered meaningful.

% PbO(wgt)	850°C	875°C	900°C	950°C	1000°C
76	0.005±0.001		0.017±0.002	0.025±0.001	0.050
77		0.0258			
78	0.0188±0.03	0.05	0.03±0.01	0.07	0.10
79		0.035	0.054		
80	0.027±0.009	0.07	0.07±0.01	0.15±0.03	
81		0.055	0.09		
82	0.037±0.01	0.11	0.126±0.008	0.25	0.40
83		0.12±0.01	0.13		
84	0.07±0.01	0.10	0.20±0.01	0.39±0.04	0.66±0.1
85		0.14	0.22		
86	0.09±0.02		0.25±0.05	0.4±0.2	0.99±0.05
87			0.49		
90	0.12±0.02			0.35	
92	0.12				

Table 2. Experimental Reaction Rates (10^{-2} cm/min).

C. Lead Oxide Mole Fraction Dependence

The relationship between reaction rates and lead oxide mole fraction is found to be linear [Fig. 9] at each temperature investigated and presents two stages corresponding to the concentration ranges 76-80% wgt. PbO and 80-88% wgt. PbO [Fig. 9].

A complementary processing of data concerning the oxidation of carbon by similar melts [Appendix 4] does not give a comparable linear dependence of the rate on PbO mole fraction.

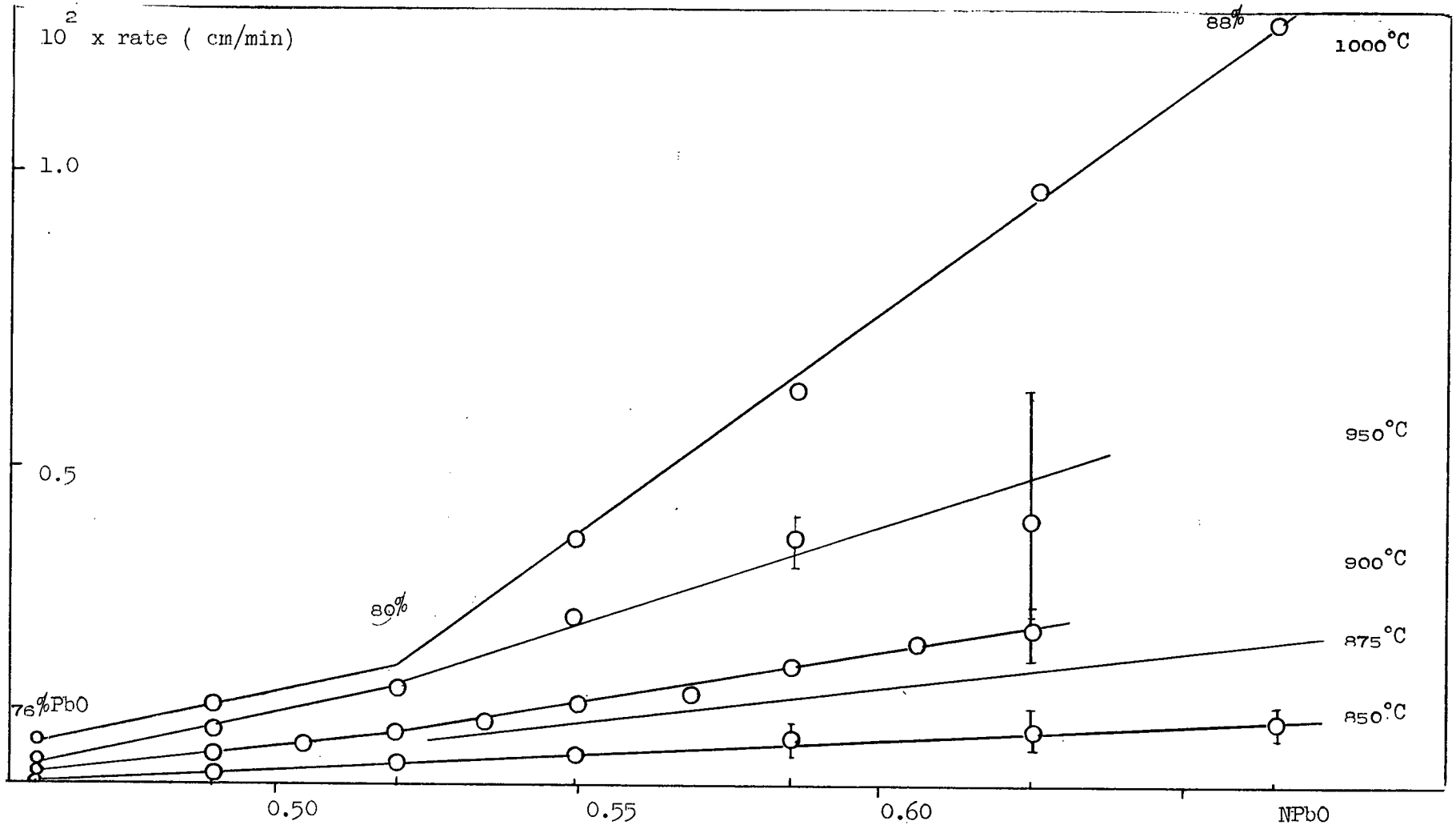

Fig. 9 : Lead oxide mole fraction dependence.

D. Oxygen Potential Dependence

In order to compare the present data with previous results concerning the oxidation of carbon by similar melts[1,2] a study of the oxygen potential dependence of the oxidation of iron follows. Preliminary considerations on the oxidation of carbon are useful for reducing the inaccuracy due to the present experimental scatter.

1. Carbon Oxidation

A processing of carbon oxidation data[1] for the concentration range 77-86% PbO is presented in appendix 4 and points out the following conclusions: (1) A log Log plot of the reaction rate versus the lead oxide activity (Fig. 24) gives an order of reaction respectively larger (2.50 for Kozuka's activity scale) and smaller (1.85 for Richardson's activity scale) than the theoretical value (n = 2) adopted by the author.

(2) On the same Log Log plot the rates observed in high silica melts (77% PbO) are lower than expected from the general dependence (Fig. 24).

(3) The linear oxygen potential dependence (rate versus $(aPbO)^2$) gives two different zero rate melts: 0% PbO on Richardson's activity scale and 72% PbO on Kozuka's activity scale (Fig. 26).

(4) The corrected Log Log plot for Kozuka's activity scale gives a linear dependence for all reaction rates (Fig. 27) the corresponding slope being reduced to 1.93.

2. Present Results

A log log plot of reaction rates versus lead oxide activity (fig.10,11) presents the following features:

(1) No general linear dependence is observed over the whole range of concentration investigated (76-88%).

(2) A linear approximation over the concentration range 78-86% gives the following slopes (reproducibility±20%):

T°C	Richardson	Kozuka
850	1.67	2.16
875	2.20	2.60
900	1.77	2.50
950	1.52	1.90
1000	1.90	2.45
average	1.81	2.22

Table 3. Reaction orders from log log plots

The mean values are close to the ones found in the preliminary study on carbon oxidation.

(3) The rates observed for high silica melts ($<$ 78% PbO) are lower than expected from the preceeding linear approximation.

Fig.10 : Log Log plots for Richardson's scale.

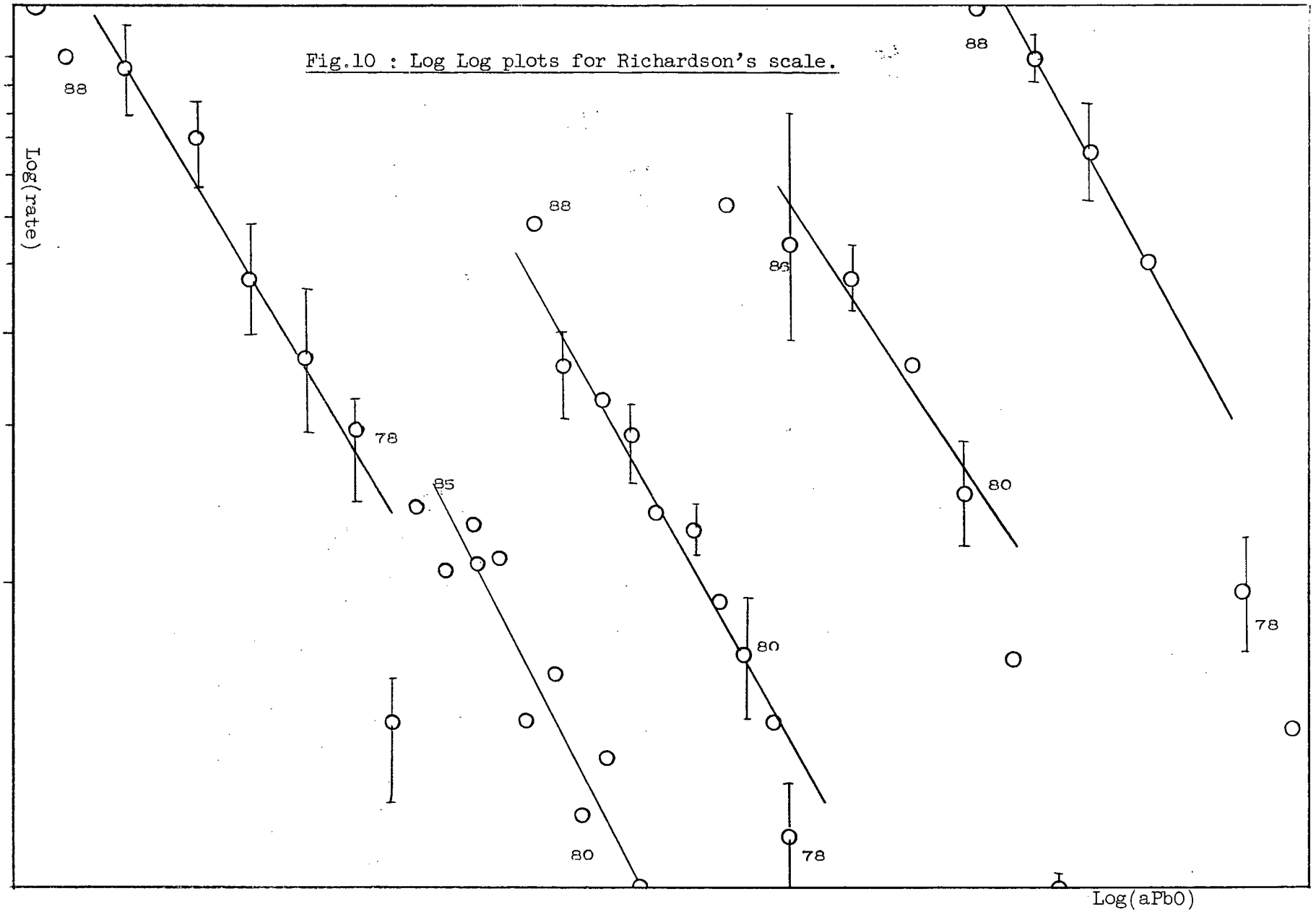

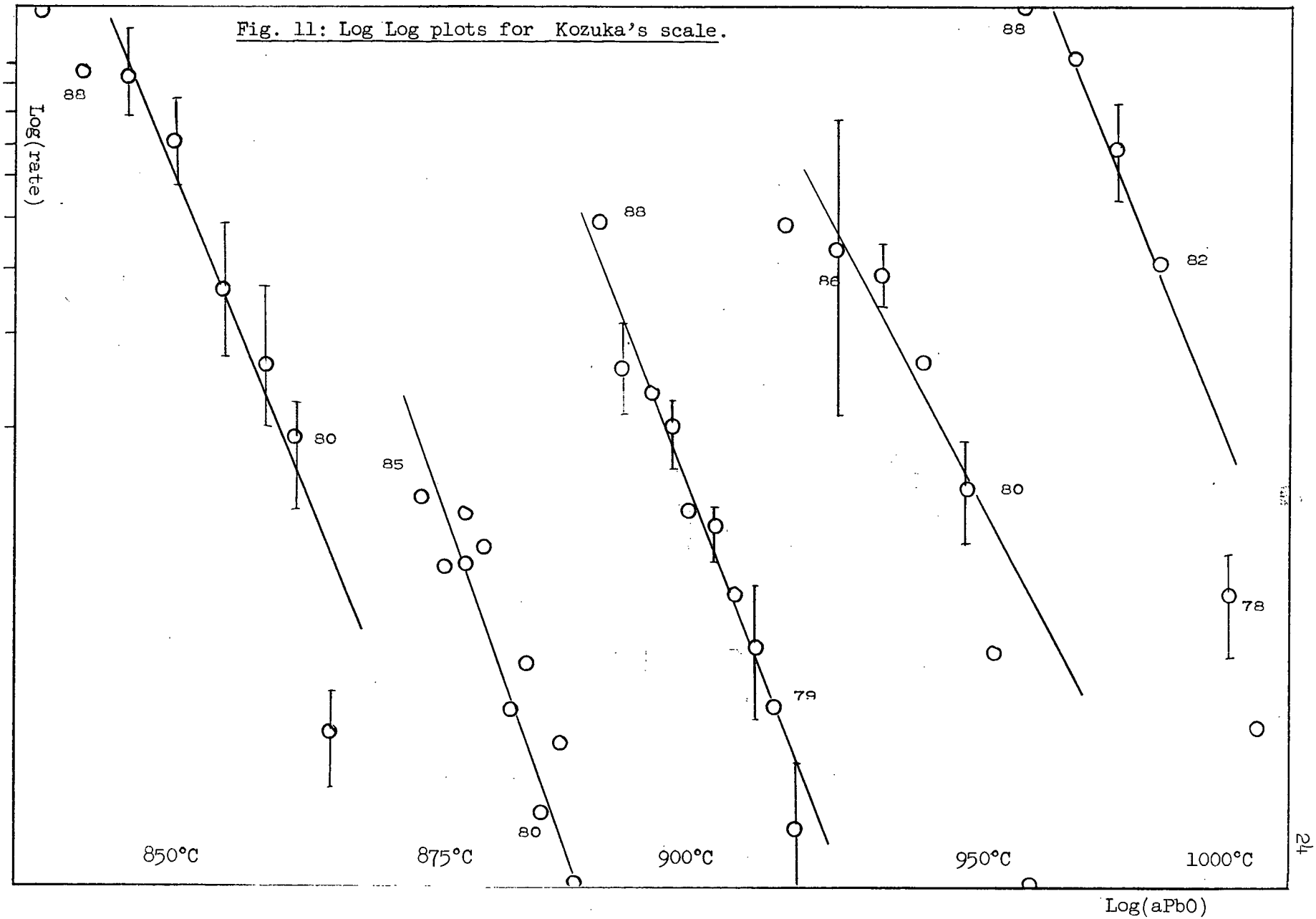

Fig. 11: Log Log plots for Kozuka's scale.

(4) A corrected log log plot for Kozuka's activity scale with a zero rate melt at 72% PbO gives a linear dependence (Fig. 12) over the concentration range 76-86% PbO. The corresponding slopes increase with temperature as shown in the following table:

°C	Kozuka (corrected)
850	2.02
900	2·16
950	2·48
1000	2·75

Table 4. Reaction order from corrected log log plots with Kozuka's scale .

The corresponding oxygen potential dependence (rate versus $(aPbO)^2$) is shown in Fig. 13 and 14. A linear approximation can be found in the concentration range 78-86% and gives two zero rate melts: respectively 0% PbO (pure silica) for Richardson's PbO activity scale and 72% PbO for Kozuka's PbO activity scale.

E. Evaluation of the Apparent Activation Energies

The activation energy of the oxidation of solid iron by $PbO-SiO_2$ melts is calculated from the curves relating the reaction rates to the melt characteristics, the slopes of these curves being the specific rate constants at the corresponding temperature.

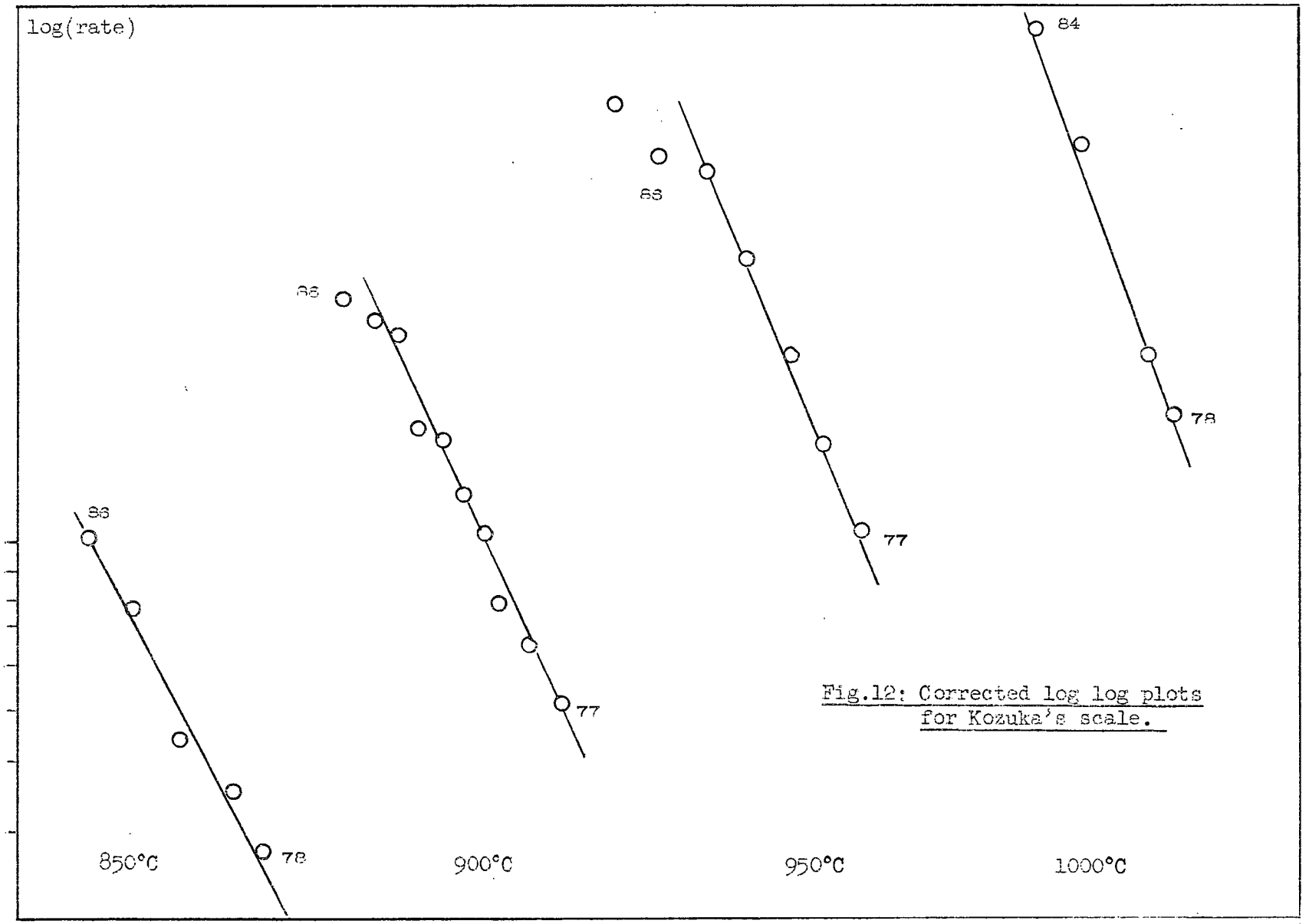

Fig.12: Corrected log log plots for Kozuka's scale.

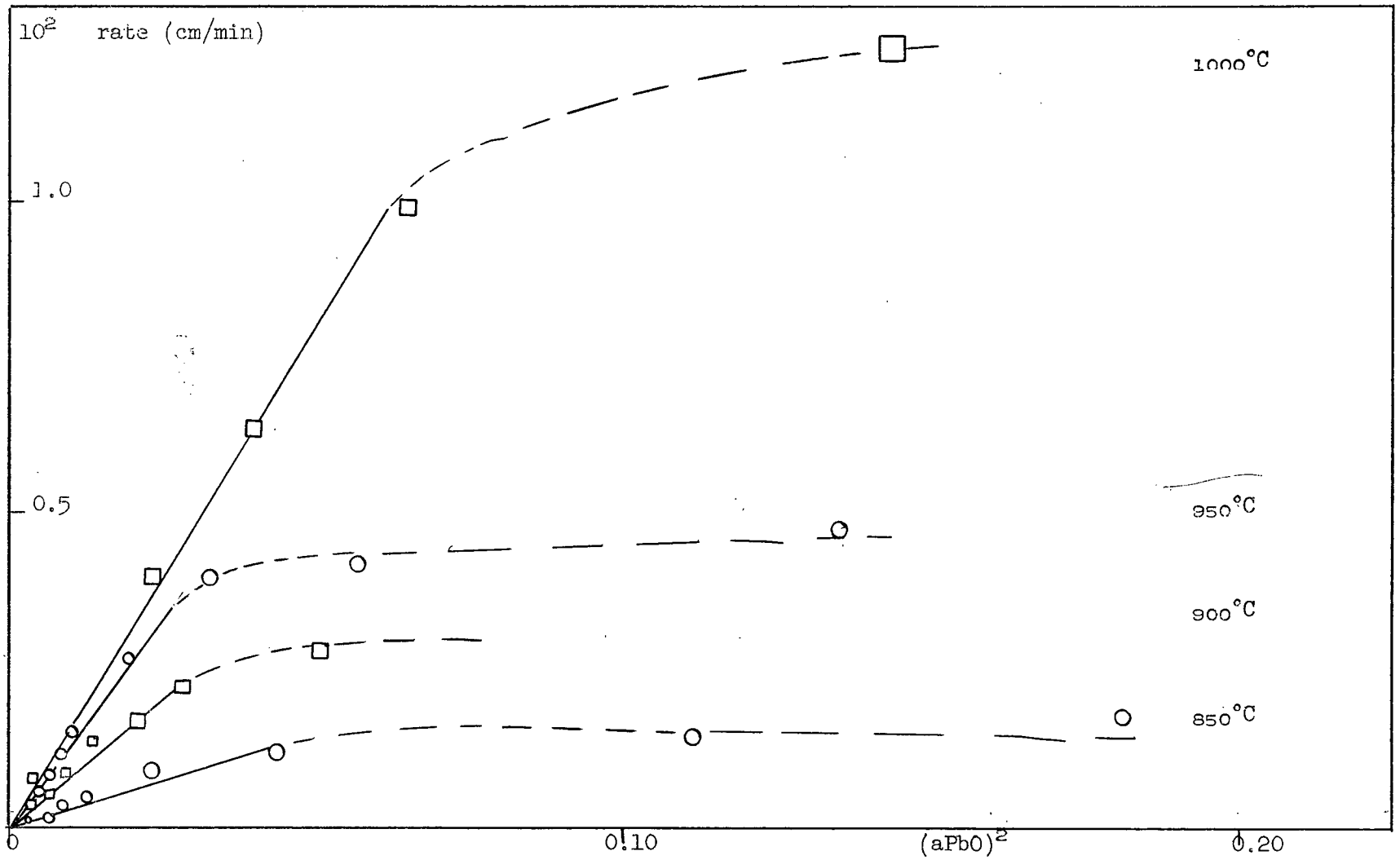

Fig. 13 : Oxygen potential dependence (Richardson's activity scale).

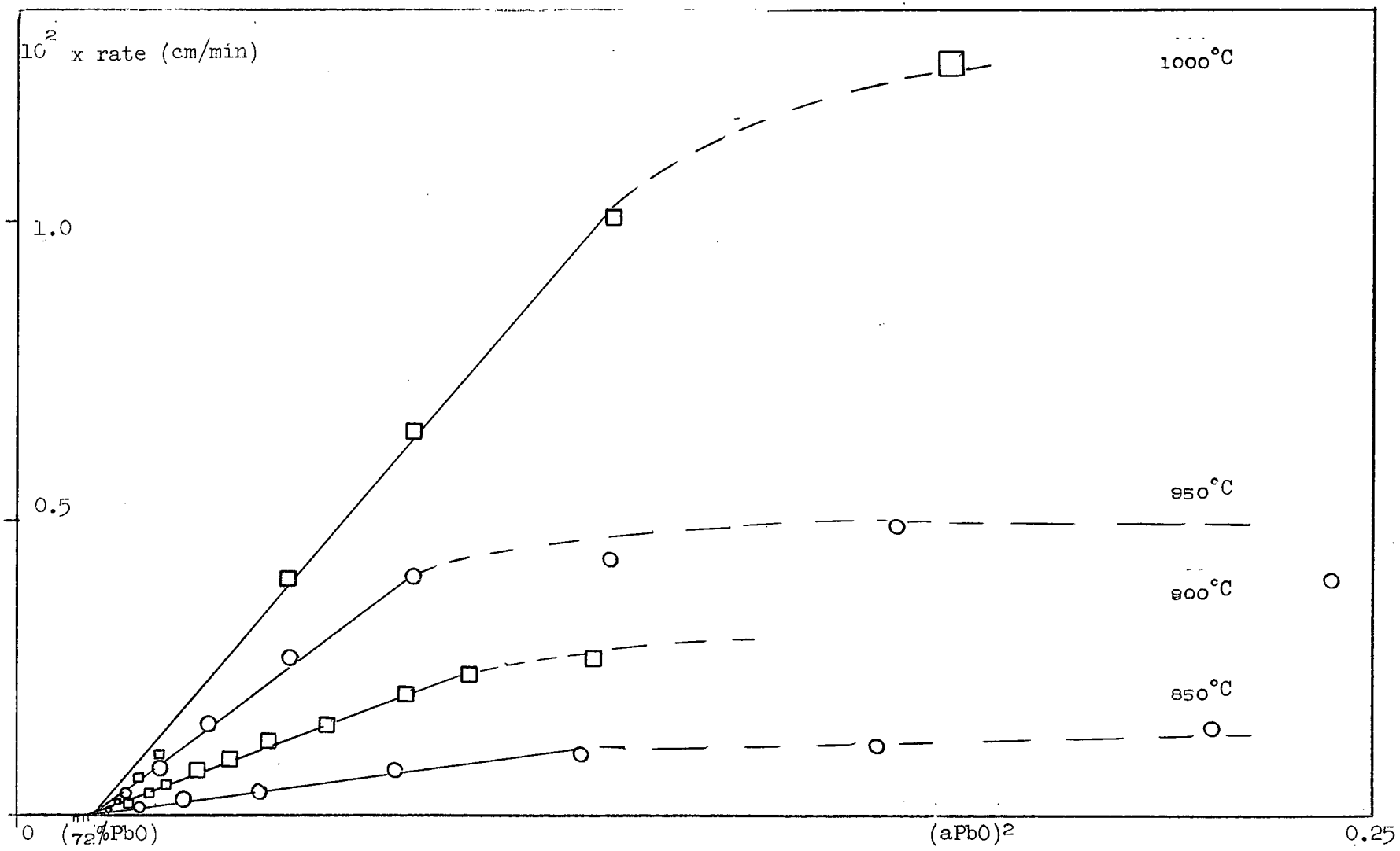

Fig. 14 : Oxygen potential dependence (Kozuka's activity scale).

[1] Pb^{++} Dependence

The Pb^{++} dependence [lead mole fraction dependence] gives an activation energy of 50 ± 7 KCal/mole [Table 5, Fig. 15], in the concentration range 80-88% wgt. PbO. In the high silica concentration range [76-80% wgt. PbO] the corresponding activation energy is found to be 36 ± 7 KCal/mole [Table 6, Fig. 16].

[2] Oxygen Potential Dependence

The oxygen potential dependence[$(aPbO)^2$ dependence] gives, by linear approximation in the intermediary concentration range [78-86% wgt. PbO], two sets of specific rate constants corresponding to the two sets of activity data [Table 7]. The corresponding Arrhenius plots [Fig. 17] give two close lines and the apparent activation energy is found to be 40 ± 10 KCal/mole.

Table 5. Specific rate constant k_1 ($gm/cm^2 x min\ xNPbO$)

°C	origin	10^2 X RATE (NPbO=0.65)	$k_1 \times 10^2$	log k_1
850	0.45	0.105	0.525	-2.28
875	0.46	0.20	1.05	-1.98
900	0.475	0.30	1.72	-1.76
950	0.475	0.55	3.14	-1.50
1000	0.50	1.15	7.7	-1.11

°C	origin	10^2x rate (NPbO=0.55)	k_2 x 10^2	log k_2
850	0.45	0.04	0.4	-3.40
900	0.448	0.1	0.98	-3.01
950	0.443	0.195	1.82	-2.74
1000	0.435	0.25	2.17	-2.66

Table 6. Specific rate constant k_2 (in high silica melts)

	Richardson's scale				Kozuka's scale			
T°C	origin	10^2rate $(aPbO)^2=.025$)	k_3x10^2	log k_3	origin	10^2rate	k_3x10^2	log k_3
850	0	0.067	2.68	-1.572	0.009	0.064	1.25	-1.903
875	0	0.139	5.6	-1.265	0.0095	0.135	2.70	-1.574
900	0	0.155	6.2	-1.208	0.010	0.178	3.56	-1.45
950	0	0.285	11.4	-0.944	0.011	0.35	7.14	-1.46
1000	0	0.42	16.8	-0.775	0.012	0.53	11.0	-0.96

Table 7. Specific rate constant k_3 (gm/cm^2x min x $(aPbO)^2$).

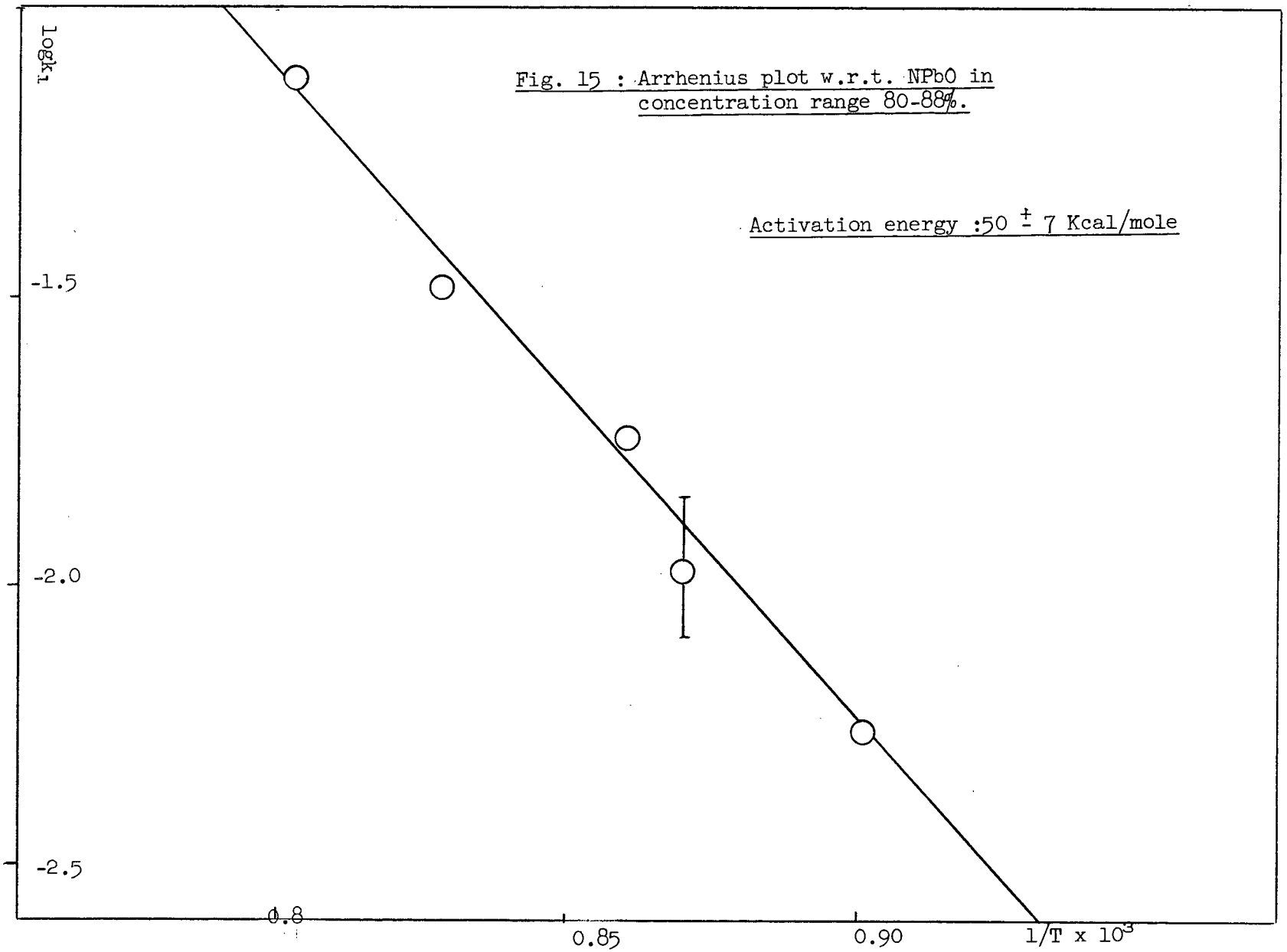

Fig. 15 : Arrhenius plot w.r.t. NPbO in concentration range 80-88%.

Activation energy :50 ± 7 Kcal/mole

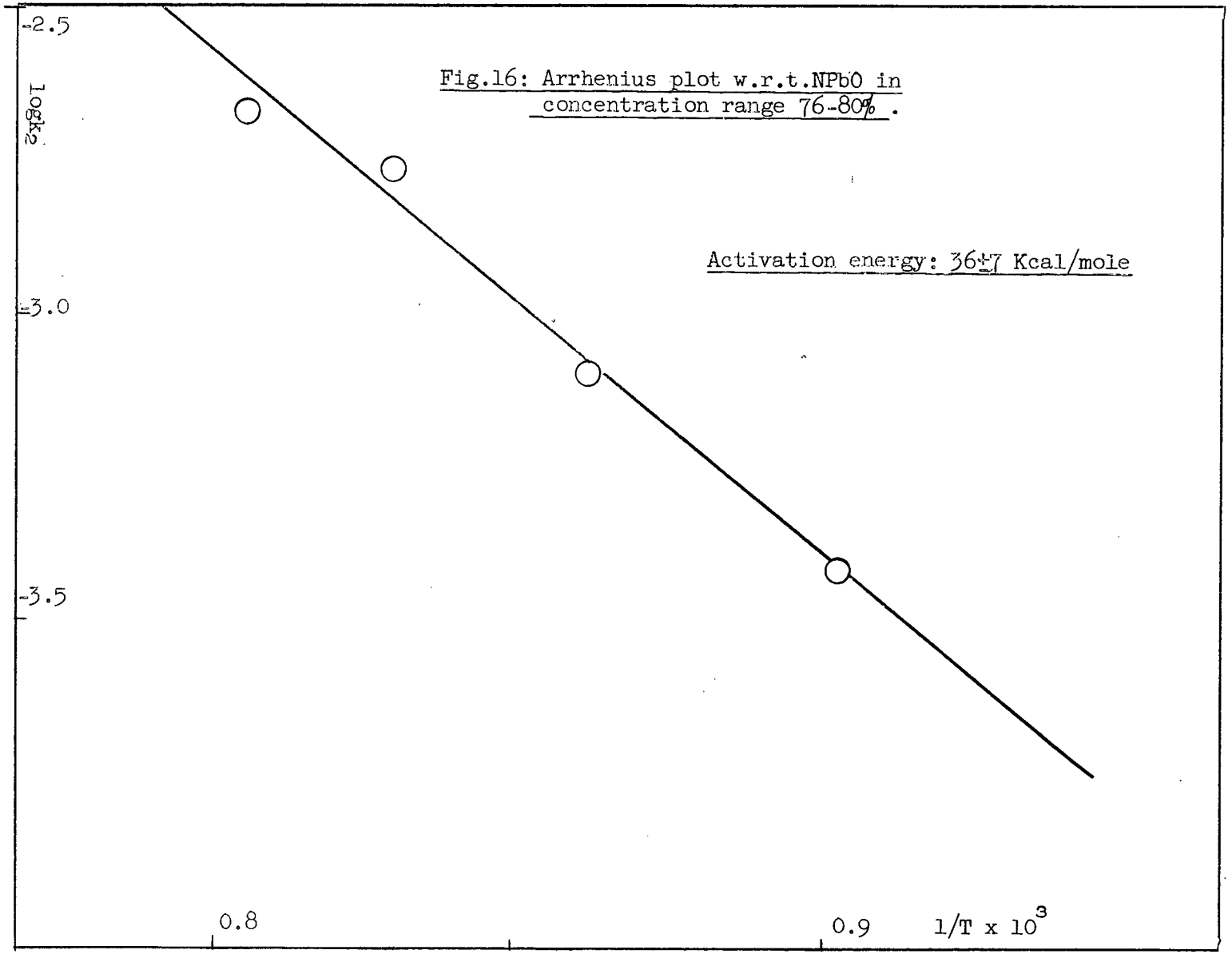

Fig.16: Arrhenius plot w.r.t.NPbO in concentration range 76-80% .

Activation energy: 36±7 Kcal/mole

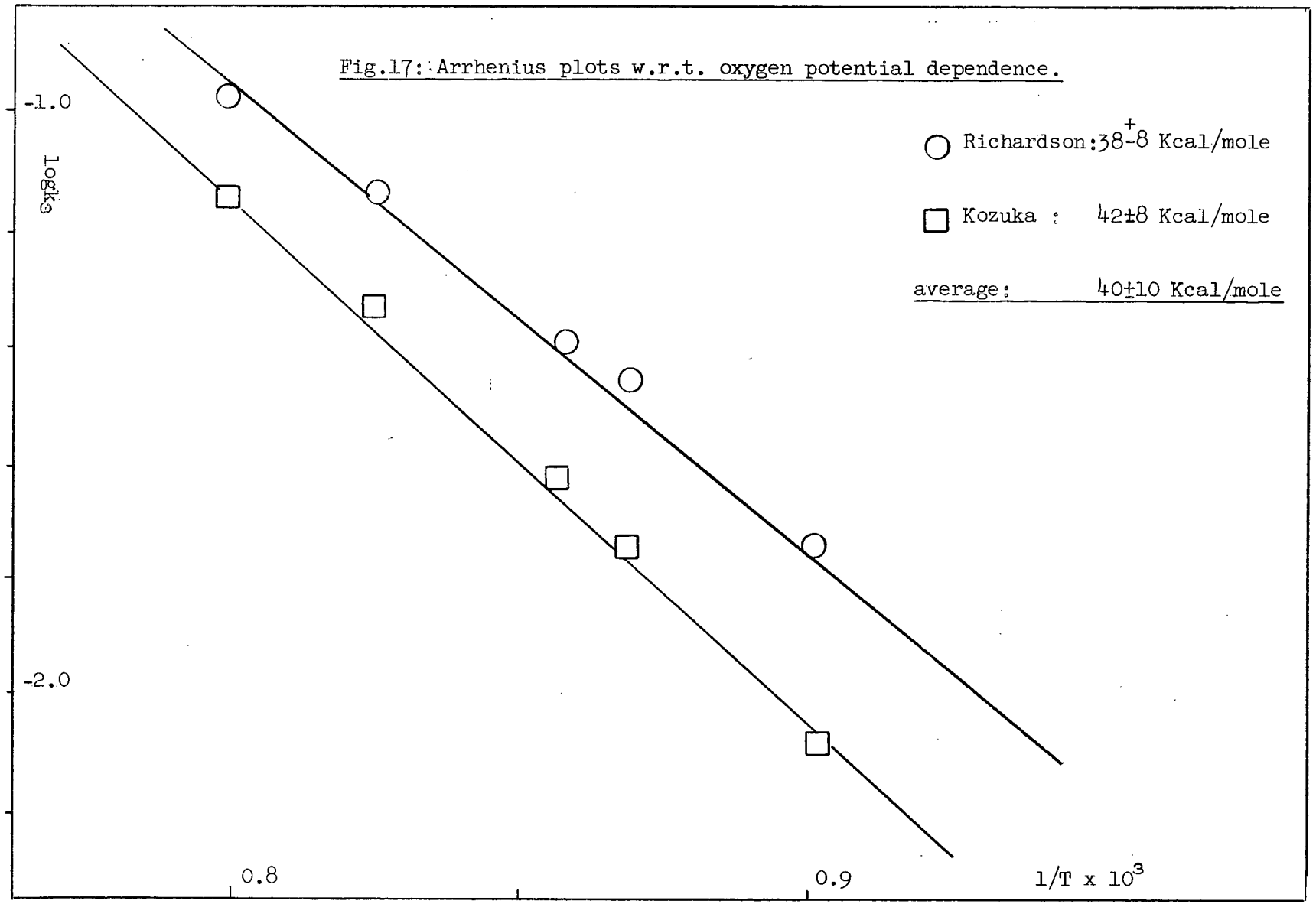

Fig.17: Arrhenius plots w.r.t. oxygen potential dependence.

DISCUSSION

A. Reproducibility

I. Observations

The basic assumption of the present experimental technique is a uniform attack of the cylindrical sample. Observations show that this is not always true:

(1) Samples observed in the course of the main linear stage present generally a uniformly reduced shape. The dispersion measured by means of a micrometer is ±5%.

(2) Samples observed in the final, non linear stage show a preferential attack in different points or in one point, all of them located in the lower parts of the sample.

A study of the error introduced in calculating reaction rates on the basis of a regular attack is presented in appendix 1 and shows that the error remains smaller than +8%.

II. Parameters

The poor reproducibility (±20%), confirmed by the above observations, is attributed to the following factors: temperature control, concentration gradient, electrochemical effect and crucible corrosion.

(1) Temperature Control

In all runs the temperature control was not better than +5 °C and -30°C. Temperature control of the furnace does not result in an accurate temperature control of the bath. The temperature measured in the

melt was generally lower than the temperature of the furnace by 10-30°C.

Direct temperature control of the melt was inaccurate for two reasons: first a variable temperature gradient (5-30°C) and convection currents exist in the melt; secondly the inertia of the Wheelco temperature controller results in a gradual shifting of the controlled temperature after any readjustement. Nevertheless, in the latter case of temperature control of the melt the temperature is more accurately known than in the first case of temperature control of the furnace.

(2) Concentration Gradient

The accummulation of reaction products results in an iron oxide concentration gradient. A vertical section of a vitrified slag shows that the slag consists of a dark brown upper part and a clear lower part corresponding to the original slag. The total concentration of iron oxide remains low ($<$ 1%) but local accummulation in the vicinity of the sample slows down the oxidation reaction.

Reciprocation of the sample did not bring meaningful improvements but too high a number of wire coils in a small space resulted in markedly lower rates.

(3) Local Electrochemical Effects

The irregular attack, more pronounced in the lower parts of the sample, is attributed to an electrochemical effect enhanced by gravity: lead droplets drip down along the sample and accummulate in the lower part of the coils, forming a local electrochemical cell.

(4) Crucible Corrosion

High lead oxide melts corrode firclay crucibles and pierce them easily.

Zirconia crucibles were tried but were given up because of susceptibility to thermal shocks.

B. Reaction Rate for a Given Melt at Fixed Temperature

Each single reaction rate curve presented two consecutive stages (Fig. 8).

(1) Initial Stage

The initial stage of low rate observed in most reaction rate curves corresponds partially to a thermal homogeneisation of the system. As could be expected from the driving force of the system, the more oxidising the melt, the smaller the length of this stage.

(2) Linear Stage

In all cases the reaction rate is proportional to the geometric surface area. Although this was true for the oxidation of carbon (1, 2), the actual experimental linear rates reported do not explicitly take into account the changing surface area of the sample, the overall linear effect being explained by means of counter-balancing factors. In the present case, the progressive decrease in the oxidising power of the melt and the production of an iron oxide gradient and an irregular attack can account for the observed linear rates which are then considered to reflect the

initial properties of the melt.

C. Lead Oxide Mole Fraction Dependence

The linear relationship between reaction rates and lead oxide mole fraction means that the rates are directly proportional to the concentration of lead cations in the melt. This implies an electrochemical step corresponding to the following reactions:

$$Pb^{++} + 2e^{-} \longrightarrow Pb$$

$$Fe \rightleftharpoons Fe^{++} + 2e^{-}$$

The reaction between Pb^{++} and the metallic phase may be considered to take place by collisions of the reactants at the same site or altternatively by consecutive electrochemical partial reactions, the sites of which need not coincide, since electrons may flow through the metal from the anodic to the cathodic sites[21]. For high Pb^{++} melts (>90%) the reaction is supposed to become controlled by the diffusional transport of cations in the melt. Similarly the slow rates observed in the concentration range 76-80% PbO where the slags are more viscous are attributed to diffusion control.

D. Oxygen Potential Dependence

In the intermediary range of concentration (78-86%) the experimental reaction rates are proportional to the oxygen potential of the binary lead silicate system. Such a dependence was found by previous studies (1, 2) on the oxidation of solid carbon. Furthermore similar results are obtained in both systems by using two sets of activity data

and by extrapolating the oxygen potential dependence to zero rate melts.

As it appears that the present system is very likely controlled by an electrochemical oxidation process involving lead cations (Pb^{++} dependence), the comparison between the activation energies of the oxidation of iron and carbon is useful for differentiating between the two systems. It would require ternary systems to distinguish between a lead ion dependence and an oxygen potential dependence.

E. Activation Energy

A comparison of the activation energies calculated by means of a rate law based on oxygen potential dependence for the oxidation of carbon and iron (Fig. 18) presents the following features:

(1) The activation energies are significantly different (22 KCal/mole and 40 KCal/mole).

(2) The values of the Arrhenius constants A are different by four orders of magnitude. This means that there is a large difference in activation entropies for the two oxidation reactions; in other words, the rate determining steps are different.

This is consistent with the model of an electrochemical process involving lead cations for the oxidation of iron in contrast to a process involving oxygen ions in the oxidation of carbon. In the latter case the oxygen ions must be involved for producing the gaseous oxidation product ($C + 2O^{--} \rightarrow CO_2 + 4e^-$) whereas in the case of iron oxidation a transfer of electrons between the two metallic species is sufficient:

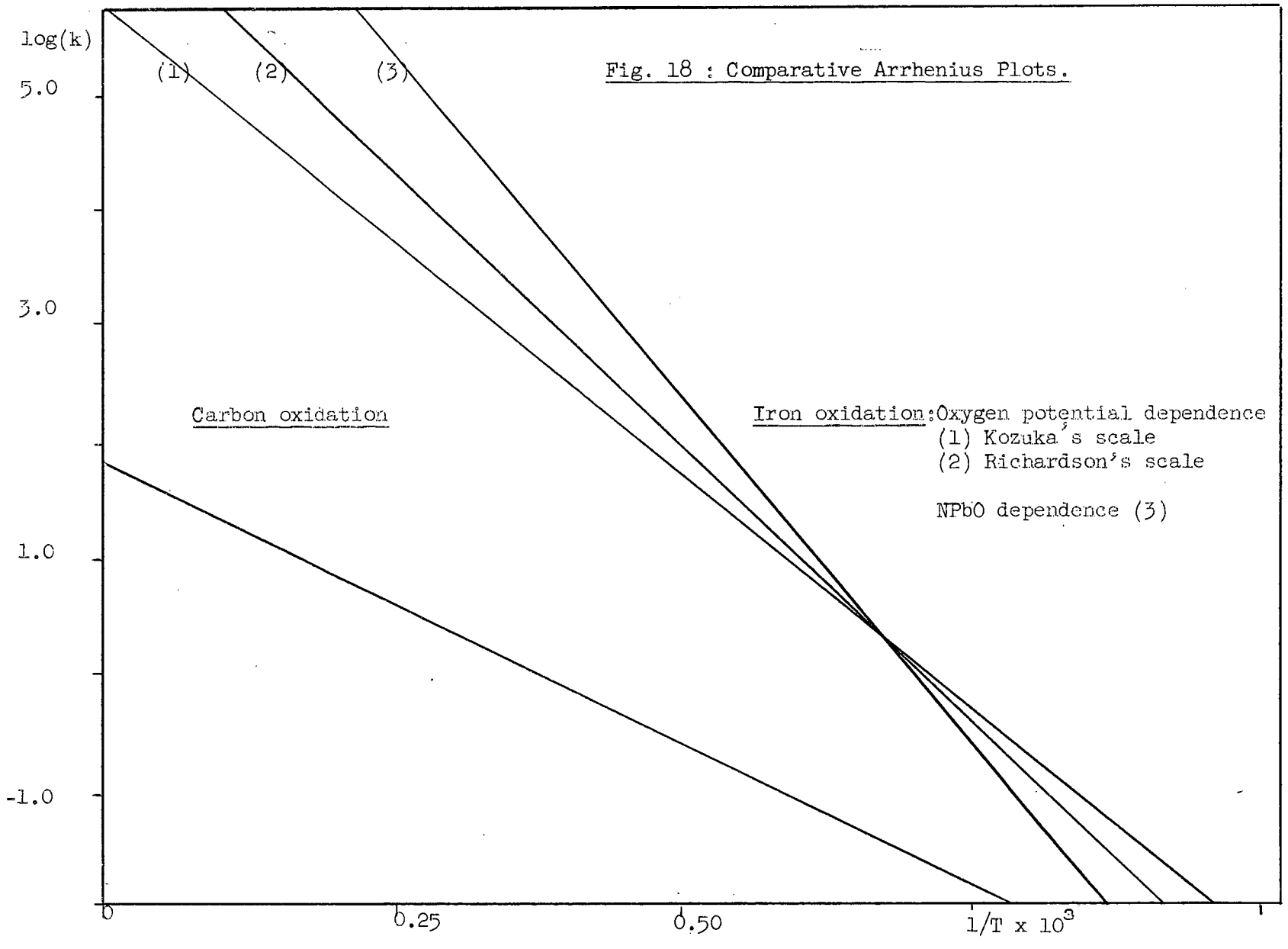

Fig. 18 : Comparative Arrhenius Plots.

$$Pb^{++} + 2e^- \longrightarrow Pb$$

$$Fe \rightleftharpoons Fe^{++} + 2e^-$$

When a rate law involving only Pb^{++} is used, the activation energy of the reaction is found to be 50 ± 7 Kcal/mole.

F. Zero-rate Melts.

A complementary study of high silica melts (70% and 73.5% wgt. PbO) shows that a reaction rate can be measured in a 73.75% PbO melt , whereas an equilibrium is rapidly reached in 70% PbO melts. A consistent zero rate melt has a composition between 70% and 73.75% PbO, as confirmed by a thermodynamical treatment of the system(appendix 5). In this connection, the processing of data relative to the oxidation of carbon and based on a oxygen potential rate law(appendix 4) resulted in two different zero rate melts: 0% PbO (pure silica) for Richardson's PbO activity scale and 72% PbO for Kozuka's scale.

In view of this and in view of the fact that Kozuka's activity scale resulted in a better fitting for the oxygen potential dependence of the oxidation of carbon, the data of Kozuka is more consistent with the investigated kinetics than the data of Richardson et al.

CONCLUSIONS

A study of the oxidation of solid iron by lead oxide-silica melts was undertaken at different temperatures. The experimental technique consisted in measuring the electrical resistance of the sample.

(1) Experimental results showed that the amount of iron oxidised per time unit was proportional to the geometric surface area of the sample.

(2) The rate of oxidation was found to be proportional to the mole fraction of lead oxide in the melt, in the concentration range 80-88% wgt. PbO.

(3) The experimental activation energy was found to be 50 ± 7 KCal/mole.

(4) By comparing the activation energy of the oxidation of iron and carbon by molten slags it is suggested that the present system is controlled in an electrochemical process by cation movements whereas the carbon system involves oxygen anions in the rate determining step.

(5) Two sets of activity data concerning the activity of lead oxide in the binary system PbO-SiO_2 are available. A complementary processing of data concerning the oxidation of carbon shows that the activity data of Kozuka are more consistent with kinetic data.

BIBLIOGRAPHY

1. Jena, P.K., M.A.Sc. Thesis, Jan. 1959, Department of Metallurgy, University of British Columbia.

2. Joshi, A.P., M.A.Sc. Thesis, Dec. 1960, Department of Metallurgy, University of British Columbia.

3. Smeltzer, W.W., Trans. Can. Inst. Min. Met. 64, 445-50 (1961).

4. Rahmel, A. and Engell, H.J., Arch. fur Eisenhuttenwesen, 30, 1459, 743-6.

5. Belin, P., Corrosion et Anticorrosion, 1960, 8, 140-56.

6. Engel, H.J., Acta Metallurgy, New York, 6 (1958), 439-45.

7. Hauffe, K. and Pfeiffer, H., Zeit. Metallde, 44 (1953) 27-28.

8. Turnbull, J.D.S., M.A.Sc. Thesis, April 1958, Department of Metallurgy, U.B.C.

9. Grigoryan, V.A., Mikhalik, E. and Ch'Ih Yung Han, Akademia Nauk SSSR, Izv. Otd. Tekhnich. Nauk Metal. i Topl., 6, (1962), 27-31.

10. Littlewood, R., Trans. AIME, 233, (1965), 772-779.

11. Ponomarenko, A. G., Teor. Prakt. Met. (Chelyabinsk) No. 7, pp. 200-9, 1964.

12. Vaisburd, S.E., and Keifers, V.L., Izv. Vys. Ucheb. Zaved., Tsvet. Metal, (1959), 2, 6, pp. 76-84.

13. Vorontsov, E.S., and Ermakov, A.V., Izv. Vys. Ucheb. Zaved., Tsvet. Metal,, 1964, 7, 4, pp. 53-9.

14. Richardson, F.D., and Webb, L.E., Trans. Inst. Mining and Met., 64, 529 (1955).

15. Kozuka, Z., and Samis, C.S., unpublished report.

16. Darken, L.S., and Gurry, R.W., Physical Chemistry of Metals, 1963, McGraw-Hill, p. 268.

17. Elliott, and Gleiser, Thermochemistry for Steelmaking.

18. Electric Furnace steelmaking , vol. II,p.248, 1963,Wiley.

19. Toop, G.W., M.A.Sc. Thesis, Sept. 1960, Department of Metallurgy. UBC.

20. Richardson, F.D., The Physical Chemistry of Steelmaking, Techn. Press of the M.I.T., 1956, p. 55.

21. King, T.B., and Ramachandran, S. The Physical Chemistry of Steelmaking, Techn. Press of the M.I.T., 1956, p. 121.

Appendix No. 1

Error on Reaction Rates

The hypothesis of a regular attack of the sample results in an approximate calculated reaction rate.

I. Definitions

M : Actual mass of unoxidised iron

r_A : Actual equivalent radius ($M = \pi r_A^2 \ell d$)

Mo: Calculated mass (assumption of a regular attack ($Mo = \rho \ell^2 d \frac{I}{V}$)

ro: Calculated radius ($Mo = \pi r_o^2 \ell d$)

α : Relative mass error ($M = Mo(1 + \alpha)$)

r_1 : Smaller radius

R : Larger radius

ℓ_1 : Irregular attack portion length

L : Specimen length

$x = \frac{r_1}{L}$ $y = \frac{\ell_1}{L}$

$E = \frac{rA-ro}{rA}$: radius error ($E = 1 - \frac{1}{\sqrt{1+\alpha}}$)

The following table gives the variations of E with α

α	0.1	0.2	0.3	0 4	0.5
E	0.05	0.08	0.12	0.15	0.18

Table 1,1.

II. Experimental Observations

"regular" attack (linear rates) : $0 < x \leqslant 0.8$

"irregular" attack (non linear rates: $0.8 < x \leqslant 2$

(the latter cases were not taken into account in reaction rate calculations).

III. Cylindrical Attack

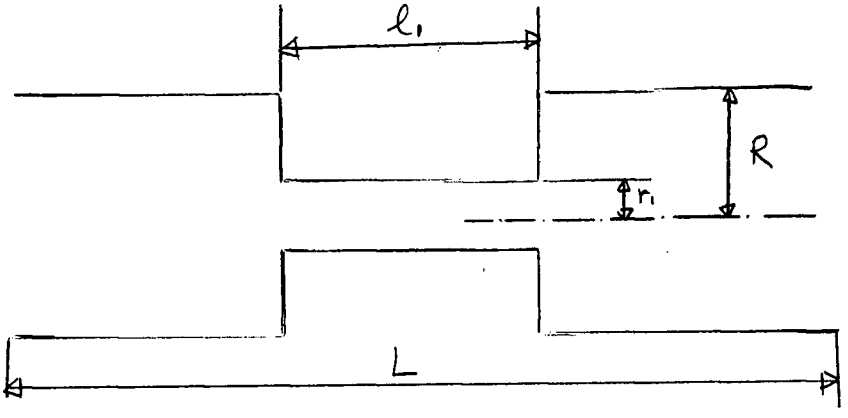

Resistance $R_1 = \dfrac{\rho \ell_1}{\pi r_1^2}$

$R_2 = \dfrac{\rho (L - \ell_1)}{\pi R^2}$

Total resistance $= \dfrac{\rho}{\pi} \dfrac{L}{R^2} \left[1 + \dfrac{\ell_1}{L} \left(\dfrac{R^2}{r_1^2} - 1\right)\right] = \dfrac{\rho L}{\pi r_o^2}$

$\therefore R^2 = r_o^2 \left[1 + y \left(\dfrac{1}{x^2} - 1\right)\right]$

Actual mass $M = \pi R^2 (L - \ell_1) d + \pi r_1^2 \ell_1 d$

$M = \pi R^2 L d \left[1 + y \left(\dfrac{1}{x^2} - 1\right)\right]$

$M = M_o \left[1 + y (1-y)\left(x^2 + \dfrac{1}{x^2} - 2\right)\right]$

$\therefore \alpha = y(1-y)\left(x^2 + \dfrac{1}{x^2} - 1\right)$

Variations of α :

x \ y	0.1	0.2	0.3	0.5
0.9	0.004	0.007	0.009	0.011
0.83	0.012	0.021	0.028	0.033
0.66	0.091	0.163	0.21	0.25
0.5	0.20	0.35	0.46	0.55

Table 1, 2

Conclusions in all cases of "regular" attack (linear rates):

$$x \leqslant 0.8 \quad , \quad y \leqslant 0.2$$

$$E < 8\%$$

IV Conic Attack

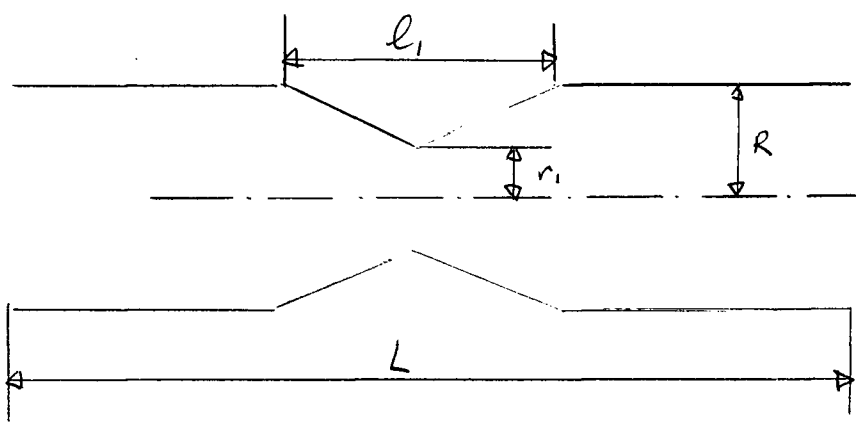

Resistance $\frac{R_1}{2} = \rho \int_0^{\frac{\ell_1}{2}} \frac{1}{\pi [r(\ell)]^2} \frac{d\ell}{} = \rho \int_0^{\frac{\ell_1}{2}} \frac{d\ell}{\pi \left[r_1 + \frac{\ell (R - r_1)}{\frac{\ell_1}{2}} \right]^2}$

$$R_1 = \frac{\rho \ell_1}{r_1 R}$$

$$R_2 = \rho (L - \ell_1) \frac{1}{\pi R^2}$$

Total resistance $= \frac{\rho L}{R^2} \left[1 + \frac{\ell_1}{L} \left(\frac{R}{r_1} - 1 \right) \right]$

$\therefore \quad R^2 = r_o^2 \left[1 + y \left(\frac{1}{x} - 1 \right) \right]$

Actual Mass $\quad M = \pi R^2 (L - \ell_1) d + 2 V\left(\frac{\ell_1}{2}\right) d$

($V\left(\frac{\ell_1}{2}\right)$ = volume of the half cone)

$$V\left(\frac{\ell_1}{2}\right) = \int_0^{\frac{\ell_1}{2}} \pi \left[r_1 + \frac{R - r_1}{\frac{\ell_1}{2}} \ell \right]^2 d\ell$$

$$V(\ell_1) = \frac{\pi}{3} \ell_1 \left[R^2 + r_1 R + r_1^2 \right]$$

$$M = \pi d L r_o^2 \left(1 + y \left(\frac{1}{x} - 1 \right) \right] \left[1 - y + \frac{1}{3} y \left(1 + x + x^2 \right) \right]$$

$$\therefore \quad \alpha = y \left[-\frac{5}{3} + y + \frac{1x}{3} + \frac{1x^2}{3} - \frac{1yx^2}{3} + \frac{1}{x} - \frac{2}{3} \frac{y}{x} \right]$$

Variations of α

Attack in one single point: $\quad x \leqslant 0.5$

$y = 0.1 \rightarrow \alpha = 0.05$

$\therefore \quad E < 5\%$

general attack with constriction in one point:

$$x \leq 0.5$$

$$y = 1$$

$$\alpha = \frac{1}{3}\left(-2 + x + \frac{1}{x}\right) = 0.16$$

$$E < 8\%$$

V Multiple conic attack

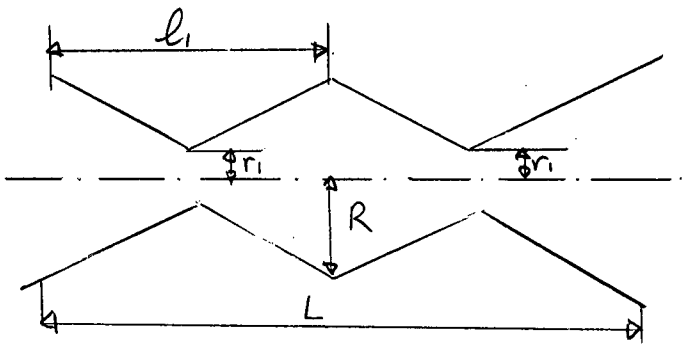

This is the precedent case with $\ell_1 \Rightarrow n\ell_1$

$$y = 1$$

$$\alpha = \frac{1}{3}\left(-2 + x + \frac{1}{x}\right)$$

$$E < 8\%$$

VI Conclusions

In all cases the error on the experimental reaction rate is inferior to 8%.

APPENDIX 1 bis

Fig. 19 : Relation between weight and mole fraction in $PbO-SiO_2$.

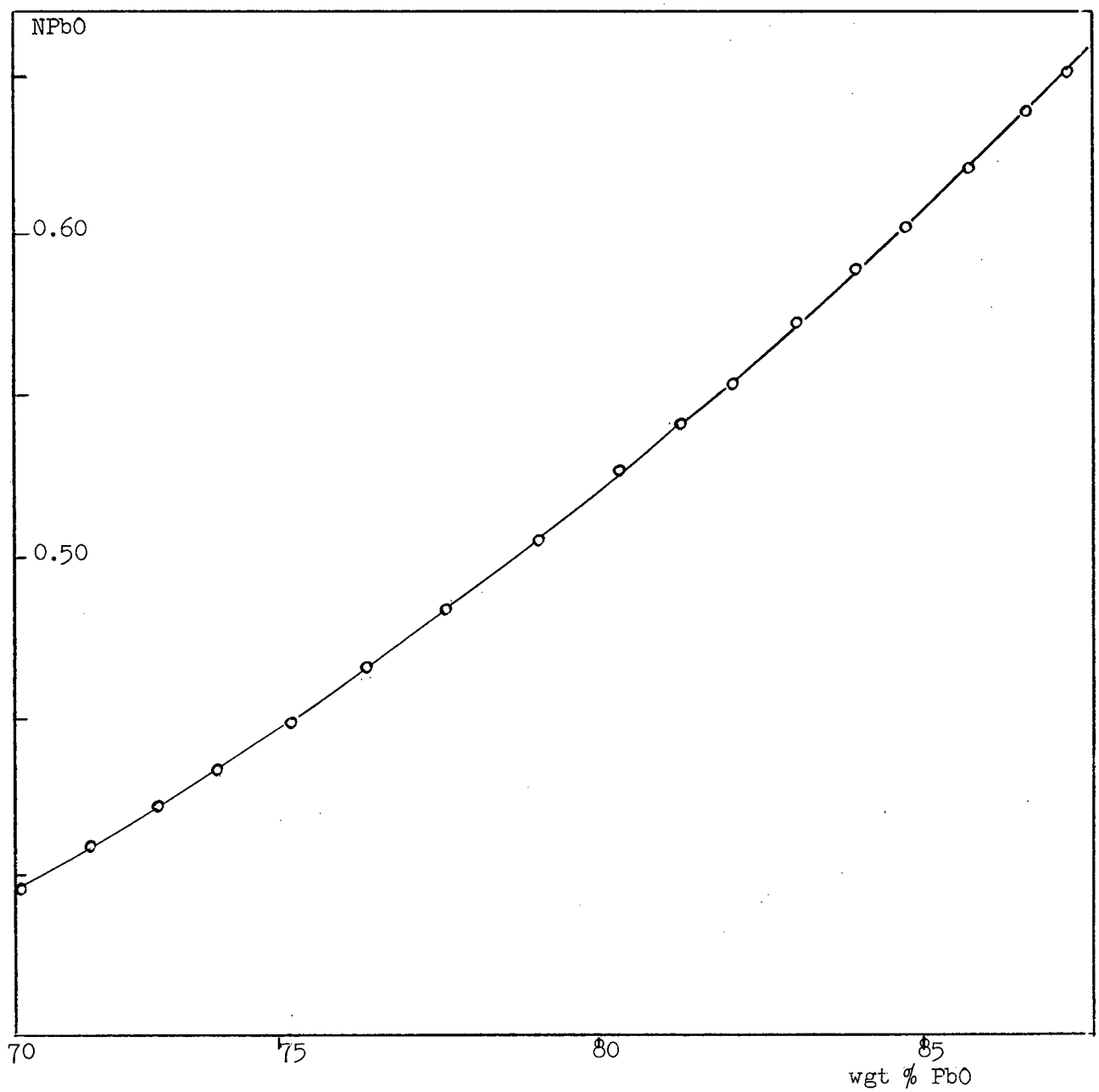

Appendix No. 2

Richardson's Activity data [14].

Richardson shows that the molten silicate PbO-SiO_2 can be considered as a regular solution in the investigated concentration range (70-95 % wgt. PbO).This is confirmed by Kozuka[15].

Therefore Richardson's data are extrapolated to lower temperatures (850, 900,950°C) by plotting log γPbO versus reciprocal temperature, since in a regular solution RTlnγ remains constant for a given mole fraction[16].

	aPbO (ref.14)			γPbO			- log γPbO		
NPbO	1000°C	1100°C	1194°C	1000°C	1100°C	1194°C	1000°C	1100°C	1194°C
0.95	0.93	0.93	0.93	0.978	0.978	0.978	0.0083	0.0083	0.0083
0.90	0.85	0.85	0.85	0.943	0.943	0.943	0.0259	0.0259	0.0259
0.85	0.76	0.76	0.76	0.893	0.893	0.893	0.0495	0.0495	0.0495
0.80	0.66	0.66	0.66	0.825	0.825	0.825	0.0839	0.0839	0.0839
0.75	0.52	0.54	0.56	0.694	0.720	0.746	0.159	0.142	0.127
0.70	0.40	0.43	0.45	0.572	0.614	0.656	0.243	0.212	0.183
0.65	0.30	0.33	0.36	0.462	0.507	0.538	0.336	0.295	0.269
0.60	0.22	0.24	0.27	0.367	0.400	0.450	0.435	0.398	0.347
0.55	0.15	0.17	0.20	0.273	0.309	0.345	0.564	0.510	0.462
0.50	0.11	0.12	0.14	0.220	0.240	0.280	0.657	0.620	0.553
0.45	0.077	0.091	0.10	0.171	0.202	0.222	0.767	0.694	0.653
0.40	0.058	0.069	0.079	0.145	0.172	0.200	0.838	0.764	0.699

Table 8. Richardson's activity data for PbO in PbP-SiO_2.

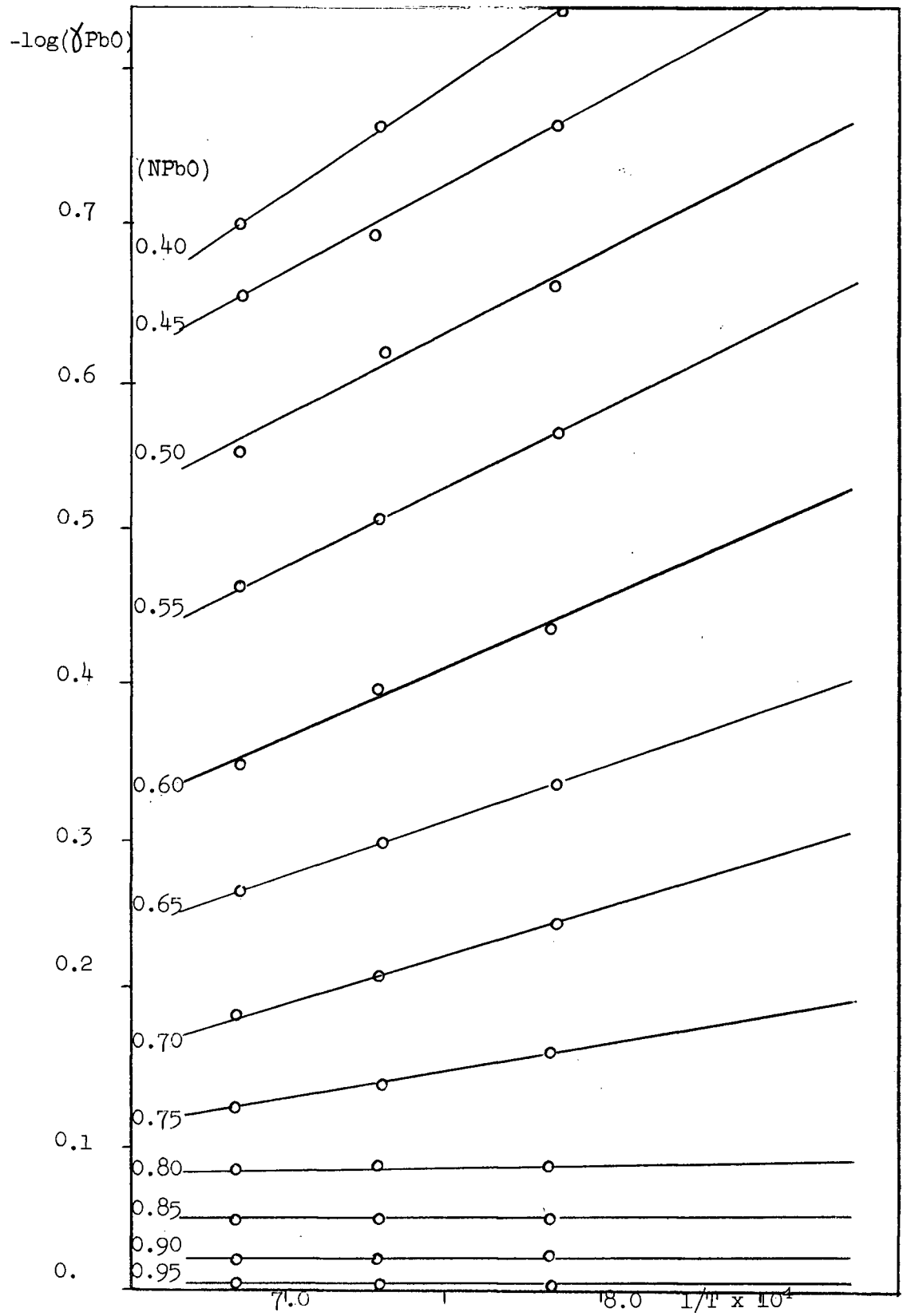

Fig. 20 : Plot of log γPbO versus 1/T (from Richardson).

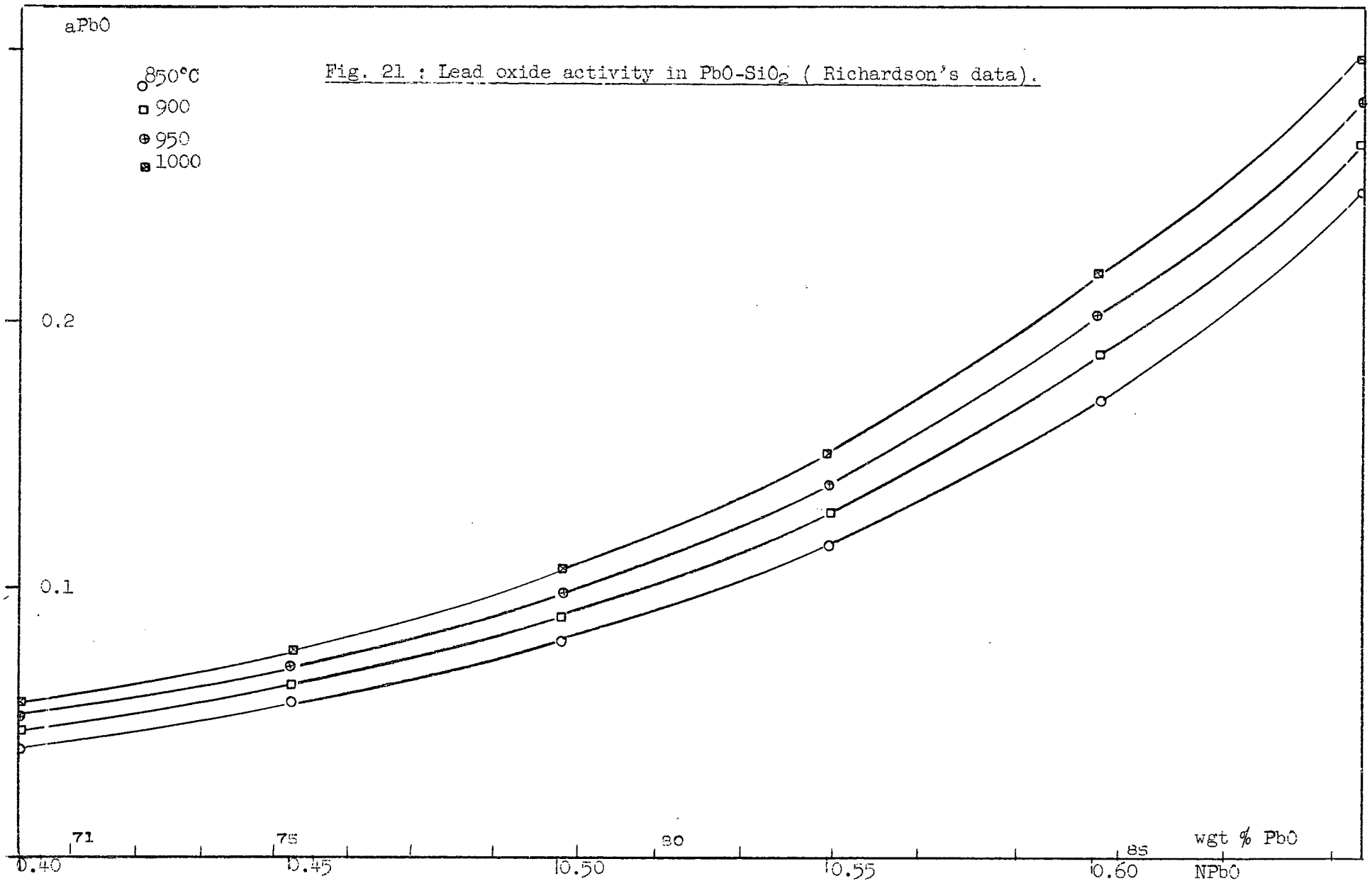

Fig. 21 : Lead oxide activity in $PbO-SiO_2$ (Richardson's data).

	- log γ			γ PbO			aPbO			
							extrapolation			ref.14
NPbO	850°C	900°C	950°C	850°C	900°C	950°C	850°C	900°C	950°C	1000°C
0.70	0.305	0.281	0.261	0.496	0.524	0.549	0.347	0.367	0.384	0.40
0.65	0.408	0.380	0.357	0.391	0.417	0.440	0.254	0.271	0.286	0.30
0.60	0.528	0.496	0.467	0.287	0.319	0.341	0.172	0.191	0.205	0.22
0.55	0.670	0.630	0.595	0.214	0.234	0.254	0.118	0.1285	0.1395	0.15
0.50	0.778	0.737	0.700	0.167	0.1835	0.200	0.0835	0.0917	0.100	0.11
0.45	0.885	0.840	0.800	0.1305	0.145	0.159	0.0587	0.0652	0.0715	0.077
0.40	0.993	0.935	0.885	0.1018	0.1152	0.1305	0.0407	0.0461	0.052	0.058

Table 9 . Activity of PbO in PbO-SiO_2 w.r.t. mole fraction.

850°C		900°C		950°C		1000°C		
aPbO	$(aPbO)^2$	aPbO	$(aPbO)^2$	aPbO	$(aPbO)^2$	aPbO	$(aPbO)^2$	%PbO
0.04	0.0016	0.046	0.0021	0.052	0.0027	0.057	0.0032	71
0.043	0.0018	0.050	0.0025	0.055	0.0030	0.060	0.0036	72
0.047	0.0022	0.054	0.0029	0.059	0.0035	0.064	0.0041	73
0.052	0.0027	0.058	0.0033	0.064	0.0041	0.070	0.0049	74
0.059	0.0032	0.064	0.0041	0.068	0.0048	0.076	0.0058	75
0.063	0.0040	0.070	0.0049	0.077	0.0059	0.084	0.0070	76
0.070	0.0049	0.076	0.0058	0.084	0.0070	0.092	0.0085	77
0.076	0.0058	0.084	0.0070	0.092	0.0085	0.102	0.0104	78
0.085	0.0072	0.093	0.0086	0.103	0.0106	0.112	0.0125	79
0.094	0.0087	0.103	0.0106	0.112	0.0125	0.123	0.0151	80
0.105	0.0110	0.115	0.0132	0.125	0.0156	0.136	0.0185	81
0.119	0.0142	0.131	0.0172	0.142	0.0201	0.153	0.0234	82
0.134	0.0179	0.149	0.0221	0.161	0.0259	0.175	0.0306	83
0.155	0.0240	0.170	0.0289	0.185	0.0342	0.200	0.0400	84
0.179	0.0320	0.195	0.0380	0.211	0.0445	0.226	0.0510	85
0.209	0.0436	0.225	0.0508	0.240	0.0575	0.256	0.0655	86
0.242	0.0585	0.260	0.0675	0.273	0.0745	0.290	0.0840	87

Table 10. Activity of PbO in PbO-SiO_2 w.r.t. wgt.% PbO.

Appendix No 3

Kozuka's Activity data[15].

Kozuka's data are extrapolated to lower temperatures (850°C) by using the linear dependence between temperature and electromotive force[15].

$nEF = -RTLnaPbO$

$n = 2$

$F = 96494$ c.

$R = 1.9872$ cal/mole x degree $= 8.3144$ joules/mole x degree.

$E \times 46121 = -4.574 \times T \times \log aPbO$

T °C	log aPbO
1273	-7.90 E
1223	-8.22 E
1173	-8.59 E
1123	-8.96 E

Table 11 . log aPbO from the emf (Kozuka's data).

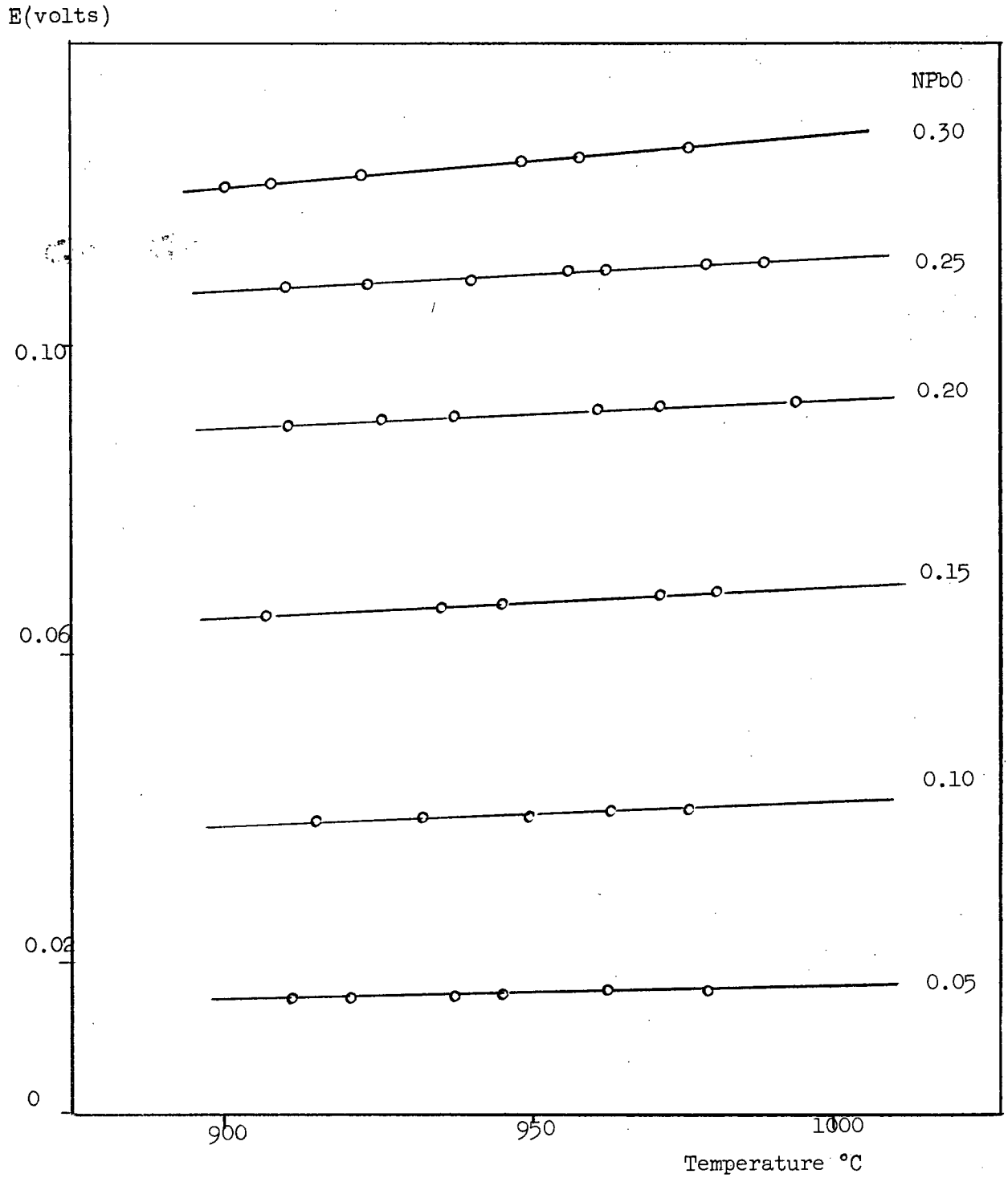

Fig.22 : Temperature dependence of the emf (Kozuka's data[15]).

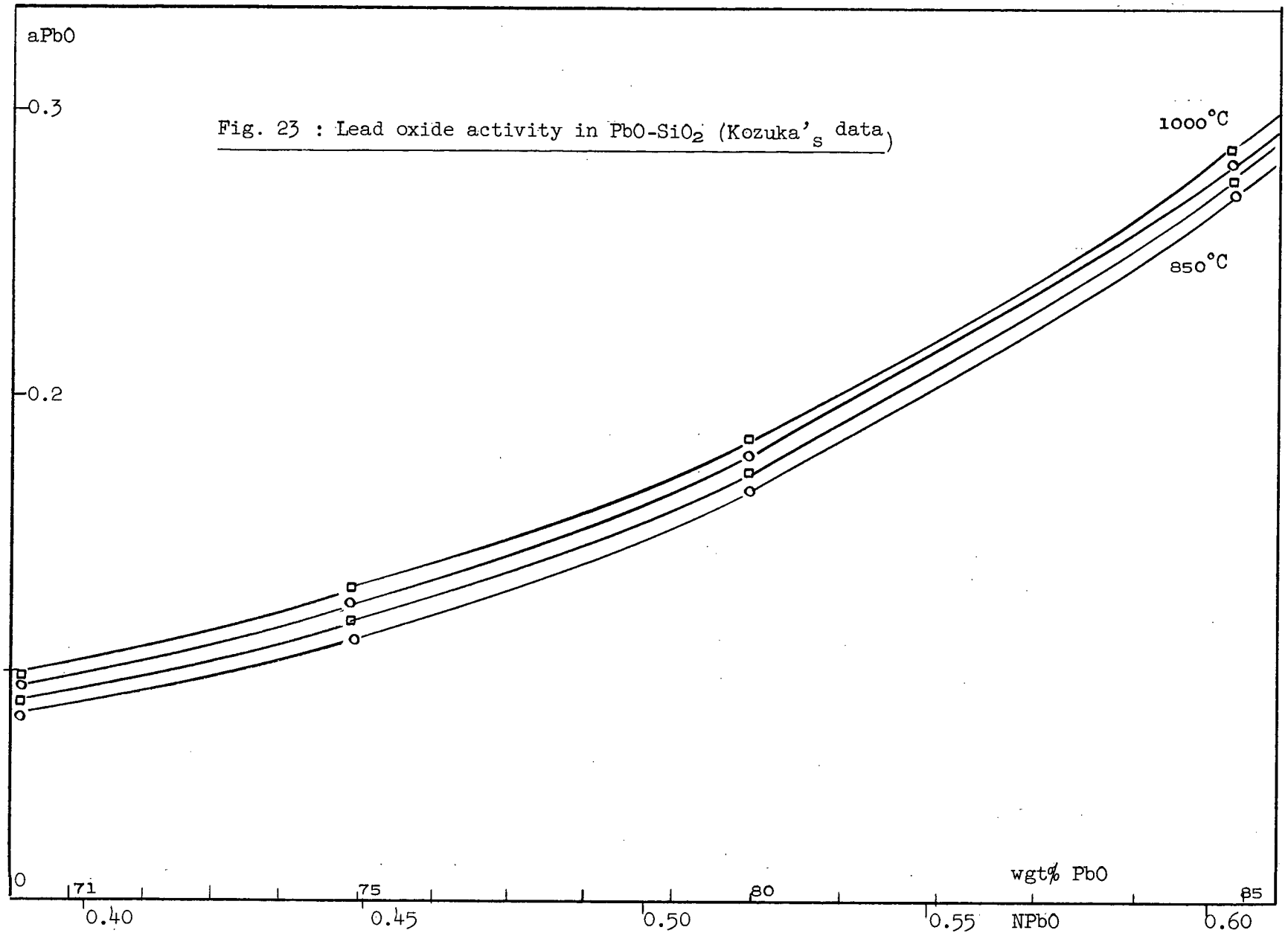

Fig. 23 : Lead oxide activity in $PbO-SiO_2$ (Kozuka's data)

	Kozuka's data			Extrapolated data		
%PbO	E	logaPbO	aPbO	E	logaPbO	aPbO
	1000°C			950°C		
5	0.0167	-0.1322	0.737	0.0157	-0.1295	0.741
10	0.0411	-0.324	0.475	0.0395	-0.3245	0.474
15	0.0687	-0.544	0.286	0.0668	-0.549	0.2825
20	0.0930	-0.735	0.184	0.091	-0.747	0.179
25	0.111	-0.877	0.132	0.1085	-0.892	0.1282
30	0.127	-1.003	0.099	0.124	-1.018	0.096
	900°C			850°C		
5	0.015	-0.129	0.743	0.014	-0.1255	0.749
10	0.038	-0.326	0.472	0.0365	-0.327	0.471
15	0.065	-0.558	0.276	0.063	-0.565	0.272
20	0.089	-0.764	0.172	0.087	-0.78	0.166
25	0.106	-0.910	0.123	0.1037	-0.93	0.115
30	0.121	-1.040	0.091	0.1182	-1.06	0.087

Table 12 . Lead oxide activity data from Kozuka.

% PbO	850°C		900°C		950°C		1000°C	
	aPbO	$(aPbO)^2$	aPbO	$(aPbO)^2$	aPbO	$(aPbO)^2$	aPbO	$(aPbO)^2$
70	0.087	0.0076	0.091	0.0083	0.096	0.0092	0.099	0.0099
71	0.089	0.0079	0.093	0.0086	0.099	0.0098	0.105	0.0110
72	0.093	0.0086	0.099	0.0098	0.105	0.0110	0.110	0.0121
73	0.099	0.0098	0.106	0.0912	0.112	0.0125	0.117	0.0137
74	0.106	0.0112	0.112	0.0125	0.118	0.0139	0.124	0.0154
75	0.114	0.0130	0.120	0.0144	0.126	0.0158	0.132	0.0174
76	0.122	0.0148	0.129	0.0166	0.136	0.0184	0.141	0.0199
77	0.131	0.0172	0.138	0.0190	0.145	0.0210	0.151	0.0221
78	0.141	0.0198	0.148	0.0219	0.155	0.0240	0.161	0.0260
79	0.155	0.0240	0.161	0.0260	0.167	0.0279	0.173	0.0300
80	0.166	0.0275	0.173	0.0300	0.179	0.0320	0.184	0.0339
81	0.183	0.0335	0.189	0.0356	0.195	0.0380	0.201	0.0575
82	0.202	0.0407	0.208	0.0432	0.214	0.0456	0.220	0.0482
83	0.223	0.0496	0.229	0.0525	0.235	0.0550	0.240	0.0575
84	0.246	0.0605	0.252	0.0635	0.258	0.0665	0.263	0.0690
85	0.272	0.0740	0.277	0.0770	0.282	0.0795	0.286	0.0870
86	0.308	0.0950	0.312	0.0970	0.316	0.100	0.320	0.102
87	0.346	0.120	0.350	0.123	0.353	0.125	0.356	0.126
88	0.375	0.141	0.380	0.144	0.385	0.148	0.40	0.160
89	0.420	0.176	–	–	–	–	–	–
90	0.470	0.221	0.470	0.221	0.470	0.221	0.47	0.221
91	0.525	0.275	–	–	–	–	–	–
92	0.580	0.336	–	–	–	–	–	–
93	0.65	0.423	–	–	–	–	–	–

Table 13. Activity of PbO in $PbO\text{-}SiO_2$ w.r.t. wgt.%
(Kozuka's data)

Appendix No 4.

Oxidation of carbon : Jena's data[1].

I. Oxygen potential.

A processing of Jena's data with the help of Richardson's and Kozuka's activity scales are presented in table 14 and fig. 24 (log log plot). The following observations can be made:

(1) The log log plot shows a linear dependence for both sets of data.

(2) The slopes are reproduced in each series of experiments.

(3) The values of the slopes are respectively larger (2.50 for Kozuka's scale) and smaller (1.85 for Richardson's scale) than the theoretical value adopted by the author (n = 2).

(4) The common point between each couple of lines corresponds to the common point of the two lead oxide activity scales at that temperature (1000°C). This point is estimated between 92 and 93 % PbO and this is confirmed in fig. 25 showing the two activity curves obtained from Richardson's and Kozuka's data.

(5) The rates observed at high silica contents (77 % PbO) are somehow lower than expected from the general linear dependendence.

The first three observations confirm the validity of Jena's conclusions concerning the oxygen potential dependence.

%PbO	10^4rate(gm/cm^{2}xmin) graphite	10^4rate carbon
77	1.00	0.79
78.8	1.63	1.17
81	2.45	1.84
82	3.13	2.24
83	3.67	2.90
84	4.80	3.68
85	6.00	4.76
86	7.90	5.85

Table 14. Jena's reaction rates [1].

The corresponding linear oxygen potential dependence (rate versus $(aPbO)^2$ is shown in fig.26 and present a significant discrepancy with respect to the zero rate melts:

Richardson's scale gives a zero rate melt at 0 % PbO (pure silica) whereas Kozuka's scale indicates 72 % PbO.

Since Kozuka's scale does not give a straight line passing through the origin a correction is necessary for the log log plot.The corrected plot (fig. 27) gives a linear dependence for all reaction rates.The corresponding slopes are reduced to 1.96 and 1.89.

II.Lead mole fraction dependence.

The corresponding plots are shown in fig. 28.

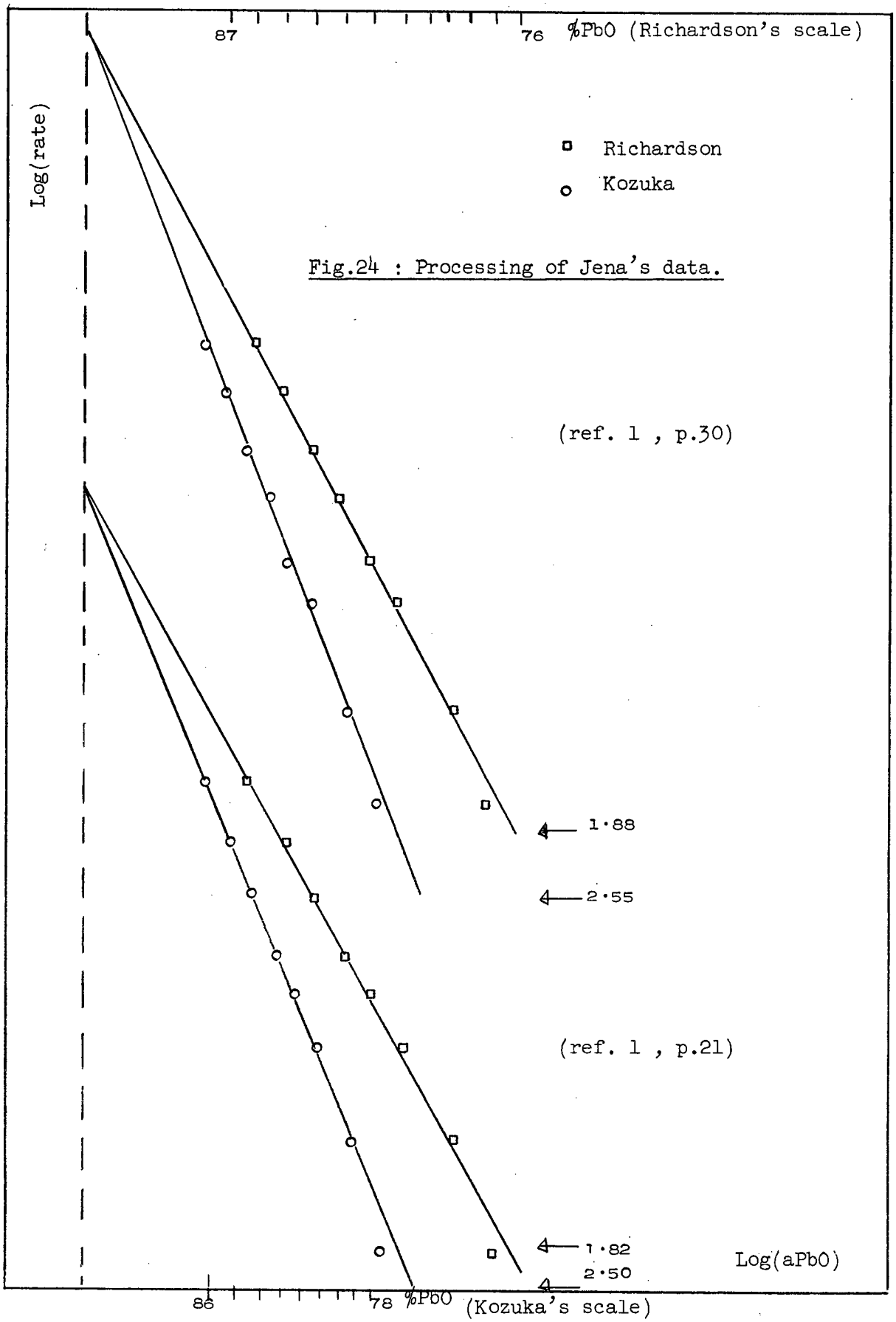

Fig.24 : Processing of Jena's data.

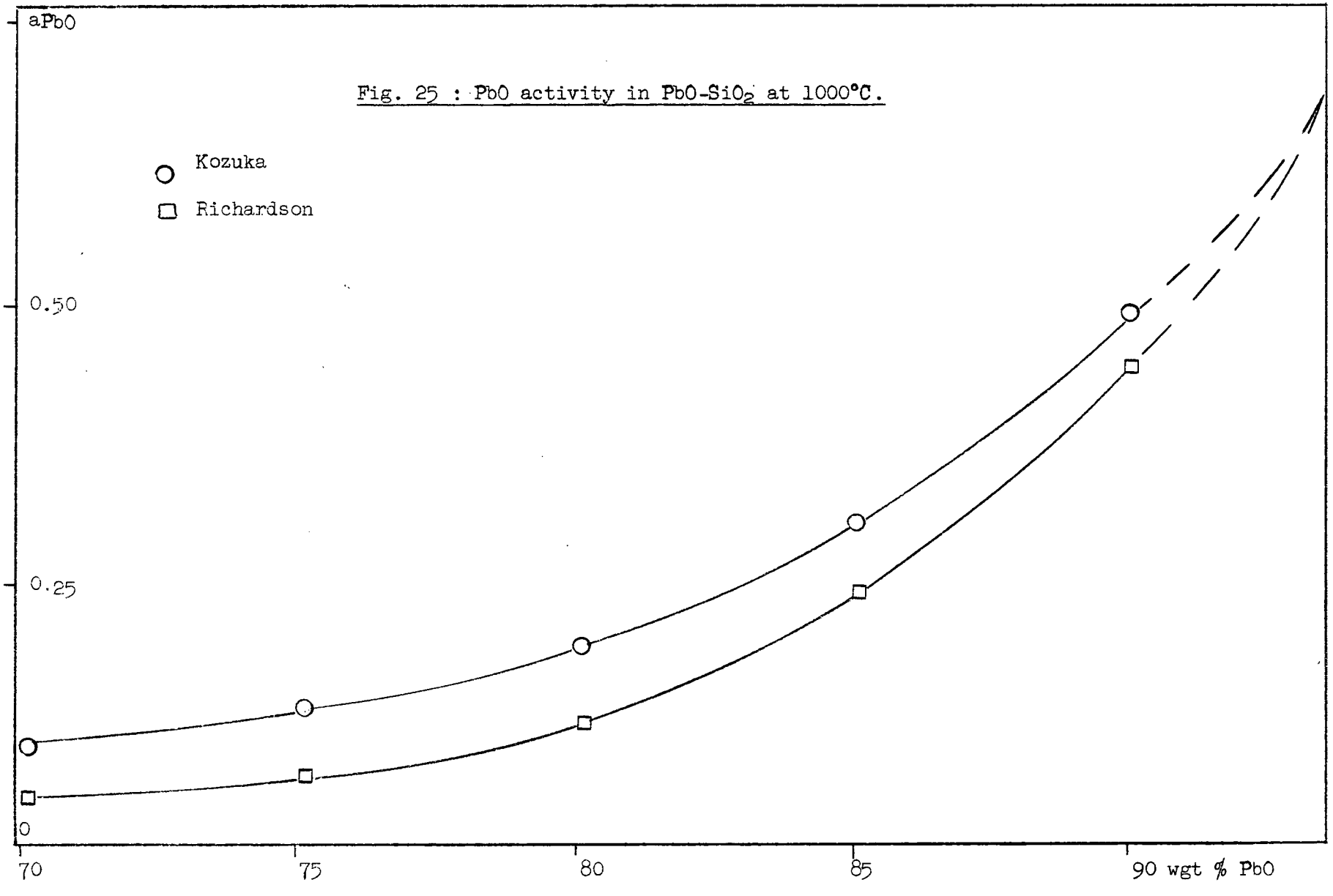

Fig. 25 : PbO activity in $PbO-SiO_2$ at 1000°C.

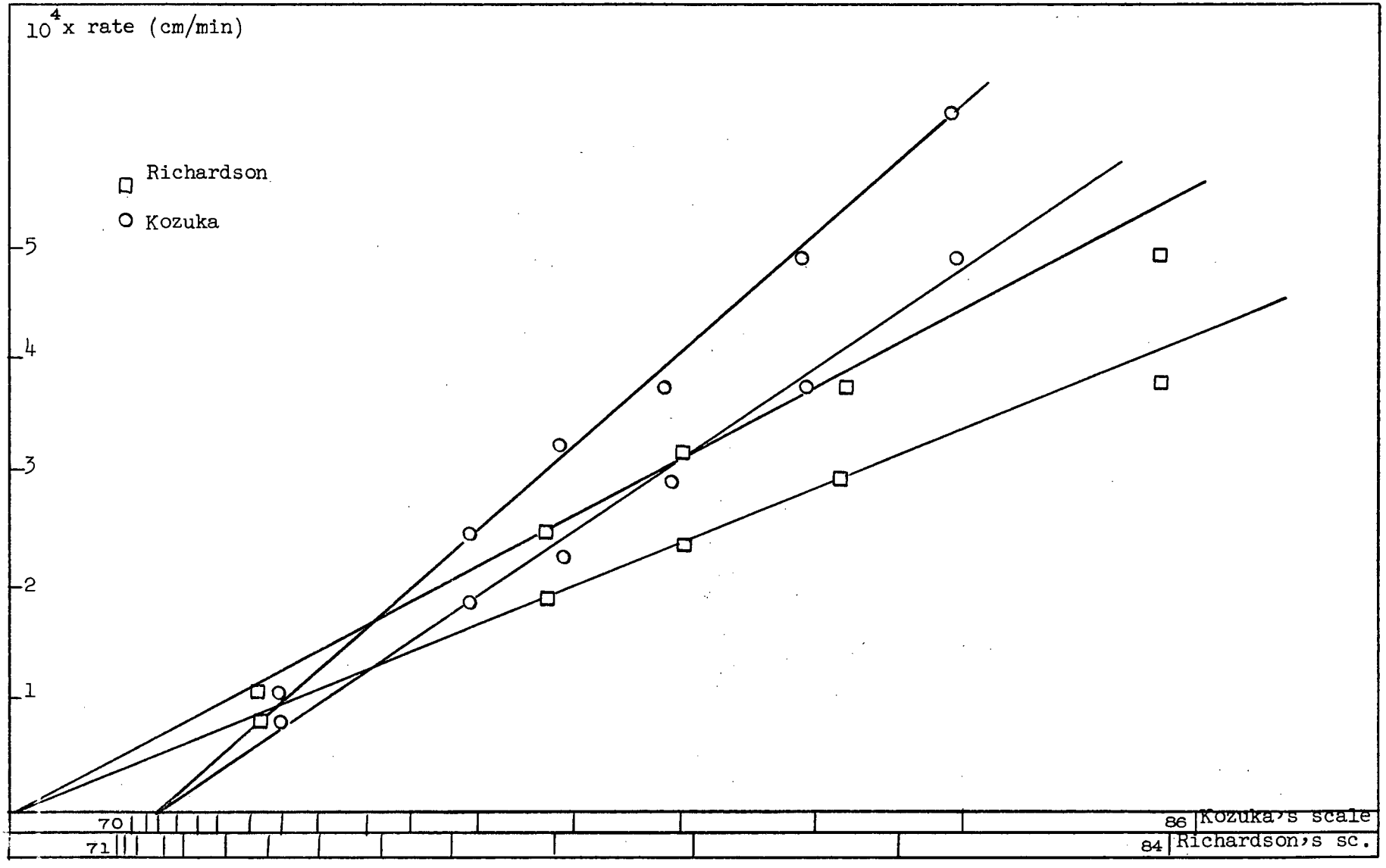

Fig. 26: Jena's results at 1000°C.

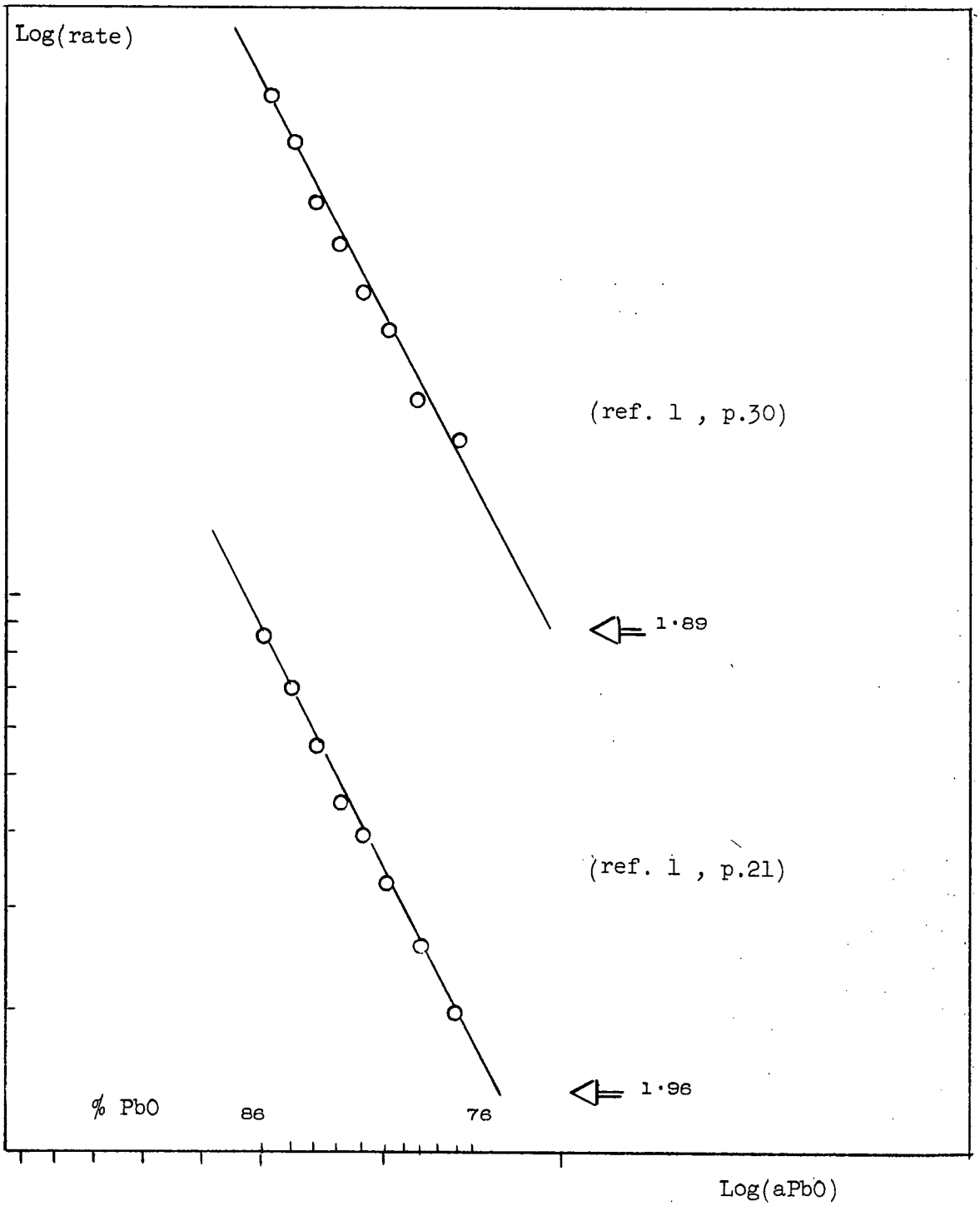

Fig. 27 : Processing of Jena's data . Corrected Log Log plot.

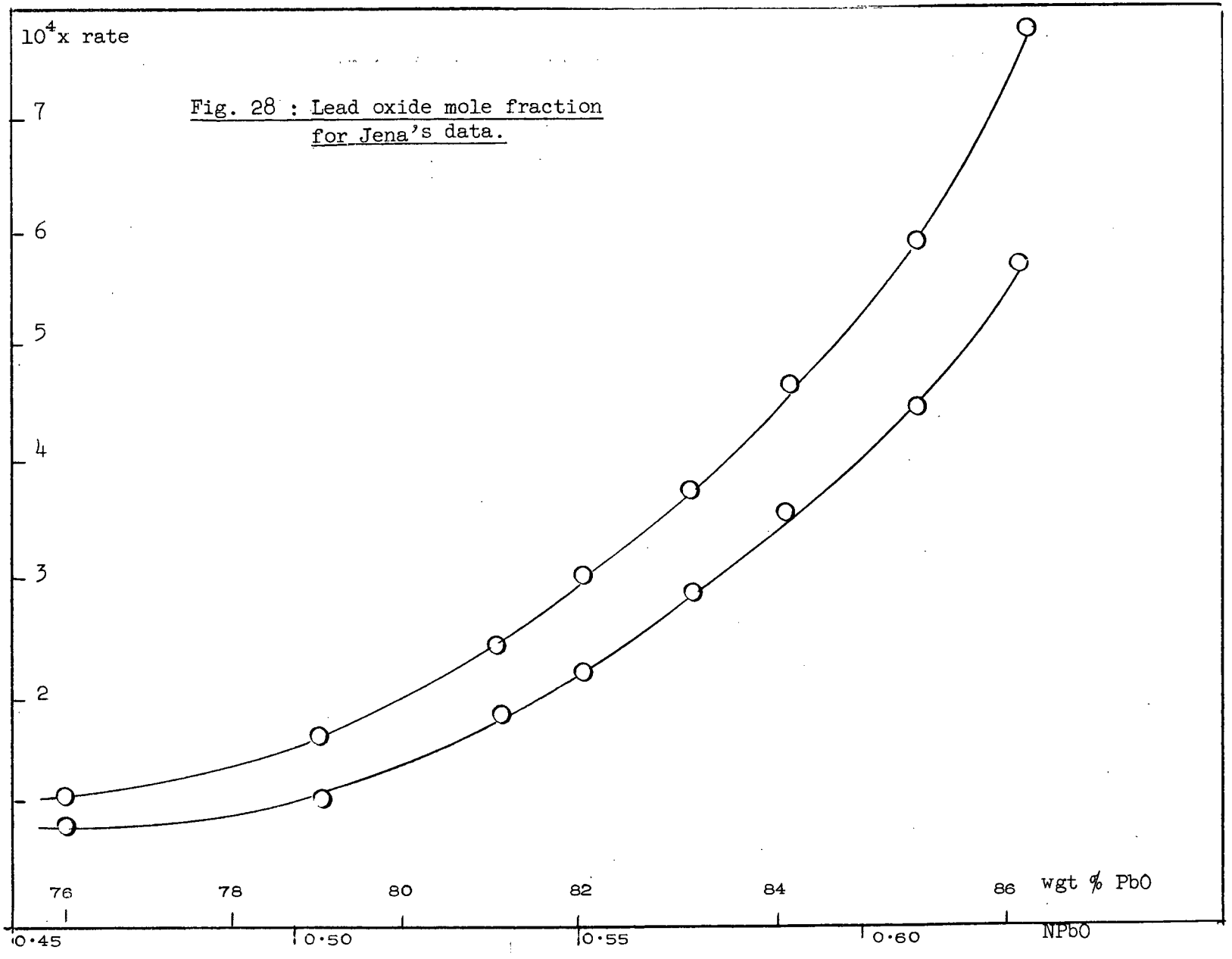

Fig. 28 : Lead oxide mole fraction for Jena's data.

Appendix No 5.

Zero rate melts

I. Thermodynamic data

For the reactions of interest :

$$Pb_{(l)} + \tfrac{1}{2} O_2 \longrightarrow PbO_{(l)} \qquad (1)$$

$$Fe_{(s)} + \tfrac{1}{2} O_2 \longrightarrow FeO_{(s)} \qquad (2)$$

$$2Fe_{(s)} + \tfrac{3}{2} O_2 \longrightarrow Fe_2O_3{}_{(s)} \qquad (3)$$

the following free energies are available[27]:

T °K	ΔF_1 cal	ΔF_2	ΔF_3
1100	-26450	-46050	-128100
1159	-25150		
1184		-44700	-123200
1200	-24450	-44450	-122200
1300	-22800	-42900	-116400

Table 15 . Thermodynamic data for the oxidation of lead and iron.

By linear extrapolation:

T °K	ΔF_1 cal	ΔF_2	ΔF_3
1123	-25750	-45650	-126700
1273	-23250	-43300	-118000

Table 16. Free energies at 1000°C and 850°C for the oxidation of Fe and Pb.

II. Oxygen Potential.

From equation (1) we can estimate the oxygen potential for a 72 % PbO melt:

$$K = \frac{aPbO}{aPb\ (P_{O_2})^2}$$

$\log K_{1123} = 5$; with aPb = 1 and aPbO = 0.086 (Kozuka):

$$P_{O_2} = 10^{-13}$$

Similarly: $\log K_{1273} = 4$; with aPbO = 0.11 (Kozuka) :

$$P_{O_2} = 10^{-10}$$

III. Zero rate point

The equilibrium between ferrous and ferric oxides

$$2\ FeO + PbO \rightleftarrows Fe_2O_3 + Pb \qquad (4)$$

gives the following equilibrium constant:

$\Delta F_{4}^{\circ}{}_{1123} = -19650$ cal

$\log K_{4}{}_{1123} = 3.8$ $\quad \therefore \quad K_4 = 6 \times 10^3 = \dfrac{aFe_2O_3}{(aFeO)^2 aPbO}$

From the value of the oxygen potential in the system one estimate approximately the ratio between the two iron oxides from a ternary diagram SiO_2-FeO-Fe_2O_3 [28]:

$$\frac{aFe_2O_3}{aFeO} \simeq \frac{1}{10}$$

hence $aFeO_{1123} \simeq 2 \times 10^{-4}$

Similarly :

$\Delta F_{4}^{\circ}{}_{1273} = -8150$ cal

$\log K_{4}{}_{1273} = 1.4$ $\quad K_4 = 25 \quad \therefore \quad aFeO_{1273} \simeq 4 \times 10^{-2}$

Conclusion: The iron oxide activies are very low in a 72% PbO melt. Therefore an equilibrium must be rapidly reached.